*Desalination and Water Treatment*
www.deswater.com

doi: 10.5004/dwt.2020.25395

185 (2020) 318–343
May

# Process optimization, isotherm, kinetics, and thermodynamic studies for removal of Remazol Brilliant Blue-R dye from contaminated water using adsorption on guava leaf powder

C. Debamita, Nakul Rampal, J.P. Gautham, P. Vairavel*

*Department of Chemical Engineering, Manipal Institute of Technology, Manipal Academy of Higher Education (MAHE), Manipal, Karnataka State, India, Tel. +91 9036270978; email: pvairavel@gmail.com (P. Vairavel), Tel. +91 9916861603; email: debamitachowdhuri@gmail.com (C. Debamita), Tel. +1-510-993-8332; email: nakulrampal@gmail.com (N. Rampal), Tel. +91 8105650199; email: gautham.jeppu@gmail.com (J.P. Gautham)*

Received 22 August 2019; Accepted 22 December 2019

**ABSTRACT**

The current batch system addresses the use of guava leaf powder as an economical adsorbent for adsorption of aromatic dye, Remazol brilliant blue-R (RBBR) from wastewater. The consequences of various experimental variables were optimized with response surface methodology (RSM) to achieve the utmost decolorization efficiency. The adsorbent was characterized by proper instrumental evaluation. Adsorption isotherms for the decolorization of RBBR were assessed by several adsorption models. The experimental equilibrium data suited the Langmuir isotherm model, and also the maximum monolayer adsorption capability ($q_{max}$) was 93.12 mg $g^{-1}$. Thermodynamic studies were performed to evaluate change in Gibbs free energy ($\Delta G$), change in enthalpy ($\Delta H$), and change in entropy ($\Delta S$) of the adsorption process. From the results, the adsorption was found to be endothermic in nature, and the process was chemisorption, spontaneous and favorable at higher temperature. Kinetic rate constants were calculated using distinct kinetic models. The dye adsorption rate followed pseudo-second-order kinetic model. The adsorption mechanisms were clarified by pore diffusion, Bangham and Boyd plots. The general rate of adsorption is controlled by both film and pore diffusion of dye compounds. Desorption studies were conducted with various desorbing reagents. Most desorption efficiency was acquired by the solvent methanol.

*Keywords:* Guava leaf powder; % Color removal; Central composite design; Kinetics; Equilibrium dye uptake; Thermodynamics; Desorption

## 1. Introduction

In the present time, environmental pollution is among the most crucial problems faced by the earth. This dilemma has steadily improved in the last few years and is now in a warning scenario [1]. Wastewater as fabric industries effluent is a substantial source of water pollution [2]. Dye effluents are believed to be one of the chief resources of acute water contamination linked to extreme color [3]. Artificial dyes often have aromatic structures and are broadly utilized in dyeing, cloth, leather, paper, pulp, plastic, rubber, cosmetic, food and pharmaceutical business. Their release as colored wastewater frequently causes pollution and ecological problems, such as the coloration of water bodies, reduction in dissolved oxygen concentration and thus kills the aquatic organisms, inhibition of sunlight penetration, loss of photosynthetic activity, and immunity to photochemical action [4]. The dye manufacturing worldwide is around 800,000 ton/y. Nearly 10%–15% of those dyes are disposed in the effluent as wastewater [5].

* Corresponding author.

The release of these effluents to water bodies has increased apprehension due to the possible health dangers connected with the entrance of carcinogenic aromatic compounds to food chains of animals and humans [6]. Additionally, the water quality of lakes and rivers has deteriorated affecting the ecosystem [7]. Nearly 45% of fabric generated globally belongs to its reactive dyes [8]. The majority of these azo dyes have been reported to be the primary cause for lung cancer in people, splenic sarcomas, hepatocarcinomas and chromosomal aberration in mammalian cells [9]. The elimination of poisonous dyestuffs out of effluents is of huge significance because of their hazardous nature in several nations globally for both water and environmental reuse concerns [10]. Thus the wastewater containing dyes have to be treated before its release from the plants.

Remazol brilliant blue-R (RBBR) is a vinyl sulphone-based formazan dye (special type of azo dye) also be known as Reactive blue 19. Based on the chromophore qualities of dyes, azo is among the major crucial groups amounting to approximately 70% [11]. Azo dyes with aromatic rings are extremely intricate and are contained in the bio-recalcitrant type of synthetic chemicals [2,6]. Additionally, RBBR possesses an intricate aromatic molecular structure character, and it could lead to bio-accumulation in the human body and aqueous ecosystem if the dye is discharged with effluent water [12]. Customary ways of removal of dyes from wastewater includes chemical filters, coagulation, electrochemical treatment, flocculation, photo-catalytic degradation, ozonation, Fenton process, sonication and biodegradation. However, these treatment technologies have different disadvantages, such as higher cost, use of new chemicals, sludge disposal issues, complex treatment processes and the requirement of substances, which can then contaminate the water [13]. Because of these constraints, there is an essential requirement for a more environmentally benign and economical method. What is more, these methods cannot be used effectively to deal with the broad variety of dye wastewater [14]. Liquid phase adsorption is commonly utilized in the elimination of noxious pollutants from effluent because appropriate design of this adsorption procedure will make a high quality treated effluent. This procedure gives an attractive choice for the treatment of polluted waters, particularly if the adsorbent is affordable [15]. Use of adsorbents for removal of dyes is better than other methods for removal of dyes due to low cost, simplicity, easy operation, stability and sludge-free functionality. In addition, this procedure is much more eco-friendly since it doesn't result from the creation of damaging substances [16]. Adsorption on industrial activated carbon was shown to be an effective procedure due to its exceptional adsorption capability and can be used to get rid of many dyes out of industrial effluents. Nonetheless, it is exceedingly costly and regeneration of spent activated carbon is comparatively hard [17,18]. To decrease the price of the treatment procedure, attention was focused on the evolution of low-cost, readily available and extremely effective adsorbents [19]. These include agricultural and plant waste materials, such as wheat bran [20], phoenix tree leaves [21], mango seed kernel [22], groundnut shell [23], neem leaf powder [24], guava leaf powder (GLP) [25], etc., which have been used for adsorbing dye from wastewater. As far as we could possibly know, no data are accessible on RBBR dye removal from aqueous solution by GLP absorbent in the literature. The present study focused on the development of an economical treatment process, the decolorization efficiency and equilibrium uptake of the untreated GLP have been studied using RBBR as a version anionic anthraquinone dye. Guava or *Psidium guajava* of the Myrtaceae family is a tropical and semitropical plant. Its leaves are multicellular, and are predominantly photosynthetic eukaryotes of the kingdom plantae. The raw leaves contain 6% fixed oil, 0.365% volatile oil, 3.15% resin, 8.5% tannin and a number of other fixed substances such as β-sitosterol, uvaol, oleanolic acid, ursolic acid, and penta cyclic triterpenoid guajanoic acid [26,27]. Its leaves and seeds have medicinal properties and are traditionally utilized to deal with a range of human disorders [26]. The goals of the current research were: to investigate the adsorption properties of GLP, to further assess the impact of various process parameters such as initial pH, adsorbate concentration, adsorbent dose, adsorbent particle size, and agitation rate, to optimize the various operating factors that are working, to ascertain the most potential adsorption capability, to examine the adsorption rate mechanism, to assess kinetics, isotherm and thermodynamic parameters and reusability of the adsorbent.

## 2. Materials and methods

### 2.1. Preparation of the adsorbent

Mature Guava leaves used for conducting the studies were collected from the Guava trees, in Kundapur, Karnataka State, India. The leaves were dried under sunlight to remove the moisture and ground to fine powder using pulverizer. The powder was then washed with distilled water. Then, the Guava leaf powder was dried in a hot-air oven at the temperature of 343 K for 8 h, ground, and screened to obtain particles <125 μm in size [25]. Dried GLP was stored in airtight plastic containers for future use. For the identification of biomass, the pictures of the dried and powdered biomass are shown in Figs. 1a and b, respectively.

### 2.2. Chemicals required

An anionic dye Remazol Brilliant Blue-R (dye content = 50%; molecular formula = $C_{22}H_{16}N_2Na_2O_{11}S_3$; molecular weight = 626.54; color index number = 61,200; CAS number 2580-78-1) supplied by Sigma-Aldrich, India was used in the study. The dye was of analytical reagent grade, and of 95% purity. All other chemicals such as sodium chloride, sodium hydroxide, hydrochloric acid, methanol, ethanol, butanol, and acetone used were of analytical grade (Merck, India).

### 2.3. Preparation of RBBR dye stock solution

The required amount of RBBR dye powder was dissolved in distilled water to prepare a 1,000 mg $L^{-1}$ stock solution. This stock solution was further diluted with pH adjusted distilled water by adding 0.1 N HCl or 0.1 N NaOH to obtain the required concentration range. After dilution (adjusting the pH), the final pH of the dye solution was measured as required range. The structure of the RBBR dye is shown in Fig. 2.


Fig. 1. (a) Dried biomass and (b) powdered biomass.

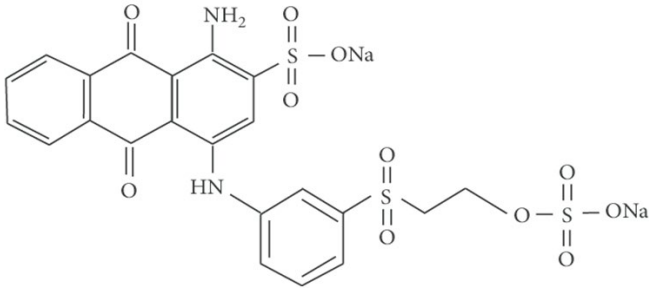

Fig. 2. Chemical structure of Remazol brilliant blue-R dye.

### 2.4. Analytical measurements

The pH of the dye solution was observed by a digital pH-meter (Systronics 335, India), and the average particle size of the GLP adsorbent was evaluated by a particle size analyzer (Cilas 1064, France). The surface area and pore volume of the adsorbent were determined using a Brunauer–Emmett–Teller (BET) surface analyzer (Smart Instruments, India). The dye concentration was measured using a pre-calibrated UV/visible spectrophotometer (Shimadzu UV-1800, Japan) at wavelength of 592 nm ($\lambda_{max}$). Attenuated transmission reflector (ATR) spectra in the transmission range of 400–4,000 $cm^{-1}$ was used to determine the functional groups in the GLP adsorbent before and after adsorption using ATR spectroscopy analysis (IR Prestige-21, Shimadzu, Japan). The surface morphology of adsorbent and RBBR dye loaded with adsorbent using field emission scanning electron microscopy/energy dispersive X-ray spectroscopy (FESEM/EDS - CARL ZEISS-FESEM attached with Oxford instruments EDS, Germany).

### 2.5. Adsorption experiments

The adsorption experiments were performed to analyse the influence of various process factors such as pH (2–12), dye concentration (50–250 mg $L^{-1}$), adsorbent dosage (1–10 g $L^{-1}$), adsorbent particle size (72–538 μm), agitation speed (0–200 rpm), and temperature (303–323 K) on the adsorptive removal of RBBR dye from wastewater using GLP adsorbent. The batch experiments were carried out by varying one factor (e.g., pH) and keeping the other factors constant. Adsorption equilibrium experiments were carried using Erlenmeyer flasks containing the known concentration of adsorbate (50–250 mg $L^{-1}$) and with fixed quantity of adsorbent dosage. The experiments were carried out in an incubator shaker at a constant speed of 150 rpm at fixed temperature till the saturation condition was attained. A known amount of solution was withdrawn at regular time intervals. Then, the samples were centrifuged (Remi CPR-24 Plus, India) at 12,000 rpm for 10 min to separate the adsorbent from the aqueous phase [28]. After centrifugation, the clear supernatant liquid was collected to analyse the residual dye concentration. The amount of CR dye adsorbed onto a unit mass of adsorbent at equilibrium and the % color removal were determined using Eqs. (1) and (2), respectively [28,29].

$$q_e = \frac{\left(C_0 - C_e\right)V}{W} \tag{1}$$

$$\%\ \text{RBBR color removal} = \frac{\left(C_0 - C_e\right)\times 100}{C_0} \tag{2}$$

where $C_0$ and $C_e$ (mg $L^{-1}$) are the liquid-phase concentrations of initial adsorbate and equilibrium, respectively, $V$ is the volume of dye solution (L), and $W$ is the mass of GLP used (g). The mean of triplicate experiments was calculated and reported.

### 2.6. Design of experiments for optimization of process parameters

Factorial experimental design (RSM) was used to obtain the overall best optimization and to minimize the number of experimental trials. It is used to investigate the relationship between % color removal and operating variables. The RSM is a widely used as a statistical method to design the experiments for optimization of process parameters. The process parameters were optimized using central composite design (CCD) to attain the maximum percentage decolorization. Factorial experimental design is used to study the effects of several factors on optimization of a decolorization process. Also, factorial designs allow measuring the interaction between each different group of factors with various levels. RSM utilizes the polynomial equation to describe the behavior of experimental data. The linear, quadratic, and interaction effects of process parameters on the response were studied with the help of the empirical model developed using RSM. The response surface method is used to (i) optimize the levels of variables (ii) examine the relationship between response variable and a set of quantitative experimental factors. Minitab 16 statistical software was employed to conduct multiple regression analysis of the data. The CCD was applied to conduct adsorption experiments. Furthermore, CCD is only applied when there is a significant lack of fit with factorial design. It also helps to find curvature in factor effects (commonly by quadratic terms). The influencing factors, such as initial pH ($X_1$), initial dye concentration ($X_2$), adsorbent dosage ($X_3$), and adsorbent particle size ($X_4$) were chosen as the independent variables. The response variables in this study are the % color removal and dye adsorption capacity at equilibrium ($q_e$). The results were fitted into the regression equation and the effect of independent variables individually and in combination was analyzed using RSM. The numbers of experimental runs are calculated by the following equation [17,30]:

$$N = 2^f + 2f + N_0 \quad (3)$$

where $f$ represents the number of variables, $2^f$ represents the number of factorial points, $2f$ represents the axial points and the center points are represented by $N_0$. A total of 31 experiments were conducted. Using $2^4$ full factorial design, we used 16 factorial points, 8 axial points, and 7 center points. The experiments were planned as per CCD with four factors at five levels. The CCD utilizes multi-level factorial design with center points, and a group of axial points that calculates the equation constants for the quadratic model. The levels of independent variables were coded as –2 (very low), –1 (low), 0 (central point), +1 (high), and +2 (very high). The coded values of process variables were obtained from Eq. (4) [30]:

$$x_i = \frac{\left(X_i - X_0\right)}{\delta X} \quad (4)$$

where $x_i$ is the dimensionless value of a process variable; $X_i$ is the real value of an independent variable; $X_0$ is the value of $X_i$ at the center point and $\delta X$ denotes the step change. The second-order polynomial equation for the relation between the independent and response variables is given as [31]:

$$Y = b_0 + b_1X_1 + b_2X_2 + b_3X_3 + b_4X_4 + b_{11}X_1^2 + b_{22}X_2^2 + b_{33}X_3^2 + b_{44}X_4^2 + b_{12}X_1X_2 + b_{13}X_1X_3 + b_{14}X_1X_4 + b_{23}X_2X_3 + b_{24}X_2X_4 + b_{34}X_3X_4 \quad (5)$$

In general, Eq. (5) can be written as

$$Y = b_0 + \sum b_i x_i + \sum b_{ii} x_i^2 + \sum b_{ij} x_i \quad (6)$$

where $Y$ denotes the predicted response variable; $b_0$ denotes the constant term (intercept value); and $b_i$, $b_{ii}$, and $b_{ij}$ denote the regression coefficients for linear, quadratic, and interaction effects, respectively. The sign of each coefficient indicates the direction of the relationship with response variable. Each coefficient corresponds to the change in the mean response per unit change in $X$ when all other predictors are held constant. The experimental ranges and levels in coded form for different factors are given in Table 1.

#### 2.6.1. Residual analysis

To verify the predicted data obtained from RSM, the predicted responses were compared with the experimental values. The root mean square error (RMSE) and the absolute average deviation (AAD) are used to predict the appropriate exactness of the model equation. The RMSE and AAD were determined using the following equations [32]:

$$\text{RMSE} = \sqrt{\left(\frac{1}{\text{N}}\sum\left(y_a - y_p\right)^2\right)} \quad (7)$$

$$\text{AAD} = \frac{1}{\text{N}}\sum\left(\frac{y_p - y_a}{y_a}\right)\times 100 \quad (8)$$

where $y_a$ is the actual response value, $y_p$ is the predicted response value obtained from the RSM, and $N$ is the number of experiments.

### 2.7. Adsorption isotherms studies

Adsorption isotherms characterize the equilibrium relationship between the quantity of solute adsorbed on the adsorbent (mg $g^{-1}$) along with the adsorbate concentration remaining in the solution (mg $L^{-1}$) in a constant temperature. The equilibrium data are necessary for designing the adsorption systems. These data provide information regarding the ability of the adsorbent and also the quantity of adsorbent required to eliminate mass of pollutant from aqueous solution under the process requirements. The isotherm models are usually analyzed from the plot of $q_e$ vs. $C_e$. The applicability and suitability of this model to the equilibrium data were measured using the values of the correlation coefficients, $R^2$, chi-square error, and $q_e$. Linear regression was carried out using the application Origin and also the technique of least squares was extensively used to ascertain the isotherm parameters [33].

#### 2.7.1. Freundlich isotherm

The Freundlich isotherm is commonly employed to model the multi-layer adsorption due to several functional groups on the surface and distinct adsorbent–adsorbate interactions (surface binding sites are unique affinities). The linear type of Freundlich model is given as in Eq. (9) [34]

$$\log q_e = \log K_F + \frac{1}{n}\log C_e \quad (9)$$

where $K_F$ is Freundlich isotherm constant (L $g^{-1}$) which indicate the relative adsorption capacity; and $1/n$ is a constant of heterogeneity. The value of $n$ is an indication of the favorability of adsorption ranging from 0 to 1. When $0 < 1/n < 1$, the adsorption is favorable; $1/n = 1$, there is no interaction among

Table 1
Experimental range and levels of independent variables for RBBR dye removal by GLP adsorbent

| Independent variables | Range and level | | | | |
|---|---|---|---|---|---|
| | –2 | –1 | 0 | 1 | 2 |
| Initial pH ($X_1$) | 1.6 | 1.8 | 2.0 | 2.2 | 2.4 |
| Initial dye concentration, mg $L^{-1}$ ($X_2$) | 100 | 150 | 200 | 250 | 300 |
| GLP adsorbent dosage, g $L^{-1}$ ($X_3$) | 1.0 | 1.5 | 2.0 | 2.5 | 3.0 |
| GLP particle size, μm ($X_4$) | 105 | 125 | 145 | 165 | 185 |

the adsorbed species; $1/n > 1$, the adsorption is unfavorable [35]. The values of $K_F$ and $1/n$ can be calculated from the intercept and slope values of the linear plot of log $q_e$ vs. log $C_e$. A high affinity of the adsorbate is described by a higher value of $K_F$ and lower value of the empirical parameter $1/n$.

#### 2.7.2. Langmuir isotherm

The Langmuir model is used for monolayer adsorption. Accordingly, in equilibrium, a saturation point is reached where no additional adsorption can happen (saturation of the available binding sites stops the adsorption of the adsorbate) [36]. The linear form of Langmuir isotherm model is given by [37]:

$$\frac{1}{q_e} = \frac{1}{q_{\max}} + \frac{1}{q_{\max} K_L C_e} \tag{10}$$

where $K_L$ is the Langmuir constant (L mg$^{-1}$) and $q_m$ is the maximum monolayer saturation capacity of the adsorbent (mg g$^{-1}$). The equilibrium parameter ($R_L$) given by Eq. (11) indicates whether the adsorption is irreversible ($R_L = 0$), favorable ($0 < R_L < 1$), linear ($R_L = 1$) or unfavorable ($R_L > 1$) [38,39].

$$R_L = \frac{1}{1 + K_L C_0} \tag{11}$$

#### 2.7.3. Temkin isotherm model

The Temkin isotherm model is expressed as [40]:

$$q_e = \frac{RT}{b_T} \ln K_T \frac{RT}{b_T} \ln C_e \tag{12}$$

where $K_T$ is the equilibrium binding constant (L g$^{-1}$), $\frac{RT}{b_T}$ is the constant related to the heat of adsorption, $b_T$ is the adsorption energy (kJ mole$^{-1}$), $T$ is the absolute temperature (K), and $R$ is the universal gas constant (8.314 J mole$^{-1}$ K$^{-1}$). The $q_e$ vs. ln($C_e$) plot is used to determine the isotherm constants $b_T$ and $K_T$ from the slope and intercept, respectively.

#### 2.7.4. Error analysis

To determine the best isotherm for adsorption of RBBR on GLP adsorbent, the chi-square ($\chi^2$) test was completed with the experimental data, to discover the very best adsorption isotherm model. In case the predicted data in the isotherm model are similar to the experimental value, $\chi^2$ will be a small number; if they are distinct, $\chi^2$ will be a sizable number. The chi-square ($\chi^2$) value was calculated with the following equation [41]:

$$\chi^2 = \sum \left[ \frac{\left(q_{e,\text{expt}} - q_{e,\text{calc}}\right)^2}{q_{e,\text{calc}}} \right] \tag{13}$$

where $q_{e,\text{expt}}$ and $q_{e,\text{calc}}$ are the experimental and predicted value of adsorption capacity of RBBR (mg g$^{-1}$).

### 2.8. Adsorption thermodynamics

The adsorption thermodynamics is vital to explore if the process is spontaneous or not and to determine adsorption behavior. Batch adsorption experiments conducted before were examined by utilizing the thermodynamic equations. The thermodynamic parameters such as Gibbs free energy change ($\Delta G$), enthalpy change ($\Delta H$), and entropy change ($\Delta S$) of this process for the adsorption of RBBR dye were determined with the following equations [29,42]:

$$\Delta G = -RT \ln\left(K_a\right) \tag{14}$$

$$\ln K_a = \frac{\Delta S_{\text{ads}}}{R} - \frac{\Delta H_{\text{ads}}}{RT} \tag{15}$$

$$K_a = q_{\max} K_L \tag{16}$$

where $K_a$ is the adsorption equilibrium constant (L g$^{-1}$), which can be graphically determined. The values of $\Delta H$ and $\Delta S$ can be determined from the slope and intercept of the Van't Hoff plot of ln $K_a$ vs. $T^{-1}$. Arrhenius equation can be used to determine the activation energy ($E_a$). The linear form of the Arrhenius equation (Eq. (17)) can be expressed as [43,44]

$$\ln K_2 = \ln A - \left(\frac{E_a}{RT}\right) \tag{17}$$

where $K_2$ is the pseudo-second-order adsorption constant (g mg$^{-1}$ min$^{-1}$) and $A$ is the Arrhenius frequency factor. The value of $K_2$ was obtained from each reaction performed at various temperatures with different concentration of adsorbate solutions and the value of $E_a$ can be determined from the slope ($-E_a/R$) of the linear plot of ln $K_2$ vs. $1/T$. The type of adsorption phenomena is generally classified as either physical [45] or chemical based on the values of activation energy and enthalpy change [46,47].

### 2.9. Kinetic studies of adsorption

An analysis of kinetics of adsorption is desired since it provides information concerning the rate-controlling step and mechanism of adsorption, which can be important to ascertain the efficacy of this process. It tracks the experimental aspects that control the rate of a chemical reaction and also the equilibrium [48]. The forecast of batch adsorption kinetics is vital for the design of industrial adsorption columns and also to create mathematical models to describe the process.

#### 2.9.1. Pseudo-first-order and second-order-kinetic models

To assess the adsorption kinetics, experimental data were fit to Lagergren pseudo first-order and Ho's second-order kinetic models, to determine the kinetic constants. The mathematical representations of both of these versions are given in Eqs. (18) and (19), respectively [49,50].

Lagergren pseudo-first-order kinetic model is given by:

$$\ln\left(q_e - q_t\right) = \ln q_e - K_1 t \tag{18}$$

where $q_e$ and $q_t$ are the solid-phase adsorbate concentrations (mg g$^{-1}$) at equilibrium and at any time $t$ (min), and $K_1$ is the rate constant of pseudo-first-order adsorption (min$^{-1}$). The values of $q_e$ and $K_1$ can be obtained from the intercept and slope of the plot of $\ln(q_e - q_t)$ vs. $t$. The linear form of pseudo-second-order kinetic equation is expressed as

$$\frac{t}{q_t} = \frac{1}{K_2 q_e^2} + \frac{t}{q_e} \tag{19}$$

The pseudo-second-order kinetic rate constant ($K_2$) is determined from the linear plot of $t/q_t$ vs. $t$. The initial rate of adsorption, $h$ (mg g$^{-1}$ min$^{-1}$) is given by Eq. (20) [51]:

$$h = K_2 q_e^2 \tag{20}$$

*2.9.2. Validity of kinetic models*

The adsorption kinetics of RBBR on GLP adsorbent was studied at various adsorbate concentrations. The kinetic model was assessed by the normalized standard deviation (SD, %), provided by the following equation [52]:

$$\text{Standard deviation}(\%) = \sqrt{\left(\sum \frac{\left[\frac{\left(q_{e,\exp} - q_{e,\text{cal}}\right)}{q_{e,\exp}}\right]^2}{N_P - 1}\right)} \times 100 \tag{21}$$

where $N_P$ denotes the number of experimental data. The best-fit model was chosen on the basis of the best $R^2$ and least SD value.

*2.10. Adsorption rate mechanism*

While designing a solid–liquid adsorption system, the dye molecule transfer and the general rate of adsorption is controlled by the slowest, rate-limiting step, which is either film diffusion or pore diffusion. The mechanism for the adsorption of dye could be presumed to involve the following five steps [53]:

- Migration of adsorbate molecules from the bulk of the solution into the hydrodynamic boundary surface of the adsorbent
- External film diffusion of dye compounds from the boundary layer into the outer surface of the adsorbent
- Adsorption of dye compounds in a binding site on the surface of solid particle
- Pore diffusion of dye compounds to the inside pores of the adsorbent particle
- Adsorption of dye compounds from the binding sites to the interior surface of the pores and capillary spaces of this adsorbent.

The diffusion mechanism of adsorption is explained by the intra-particle diffusion model. This model is represented with the following Weber and Morris equation (Eq. (22)) [54]:

$$q_t = K_i t^{0.5} + C \tag{22}$$

where $K_i$ is the intra-particle diffusion rate constant (mg g$^{-1}$ min$^{-1/2}$) and $C$ is the constant. The thickness of the boundary film is given by the value of $C$. The values of $K_i$ and $C$ are determined from the slope and intercept, respectively, of the linear plot of $q_t$ vs. $t^{1/2}$. The intercept of the plot reflects the extent of the of boundary layer effect. The Boyd and Bangham kinetic expressions were used to predict the rate-determining step. These two kinetic expressions are described by the following equations [55,56]:

Boyd kinetic expression:

$$F = 1 - \left(\frac{6}{\pi^2}\right) \exp\left(-B_t\right) \tag{23}$$

(or)

$$B_t = -0.4977 - \ln(1 - F) \tag{24}$$

$$F = \frac{q_t}{q_e} \tag{25}$$

where $F$ is the ratio of solute adsorbed at any time $t$, and $B_t$ is a mathematical function of $F$.

Bangham kinetic expression:

$$\log\left(\log\left(\frac{C_0}{\left(C_0 - q_t m\right)}\right)\right) = \log\left(\frac{k_0 m}{2.303V}\right) + \alpha \log t \tag{26}$$

where $m$ is the weight of adsorbent used per liter of solution (g L$^{-1}$), $\alpha$ is a constant and $k_0$ is the Bangham constant (L$^2$ g$^{-1}$).

*2.11. Desorption studies and reusability of the adsorbent*

Desorption experiments have been conducted with various desorbing reagents, for example, methanol, ethanol, acetone, and 1 M NaOH in separate batches to explore the prospect of retrieval of the adsorbent [20]. In a normal desorption experiment, 100 mL of above-mentioned desorbing reagents are added into the adsorbent filled with adsorbed dye molecules and agitated for a sufficient period in separate batches. The procedure is continued until the dye has been desorbed by the desorbing reagent, after that the centrifugation process was utilized to separate the regenerated adsorbent and desorbed dye compounds. To be able to establish the trustworthiness of the adsorbent, successive adsorption–desorption cycles were replicated three times using exactly the same adsorbent. The desorption for the second and third runs was carried out using 100 mL of this above-mentioned assortment of reagents in separate batches. The regenerated adsorbent after desorption was collected by centrifugation and was then left to dry at 343 K for 8 h. The % color removal of this regenerated adsorbent was analyzed in second and third runs beneath the optimized values of this process factors and compared with the initial run. The efficacy of desorbed dye from the adsorbent was determined using the following equation [41]:

$$\text{Desorption efficiency} = \frac{\text{Concentration of RBBR dye desorbed}}{\text{Concentration of RBBR dye adsorbed}} \times 100 \tag{27}$$

## 3. Results and discussions

### 3.1. Characterization of the GLP adsorbent

The specific surface area and pore volume of the GLP were analyzed based on the nitrogen adsorption at 77 K. The BET surface area of the adsorbent was 1.9 $m^2 g^{-1}$. The pore volume was measured as 1.5 $mm^3 g^{-1}$, with an average particle size of 104.13 μm. The Methylene blue (MB) index was tested to calculate the Methylene blue number using standard operating procedure. The MB number is defined as the maximum amount of dye adsorbed by 1 g of adsorbent at an equilibrium concentration [57]. Its value was calculated to be 24.658 mg $g^{-1}$ with MB, and GLP adsorbent concentration of 100 mg $L^{-1}$, 2.5 g $L^{-1}$, respectively, at pH 9. Furthermore, iodine number (amount of iodine adsorbed per gram of adsorbent at an equilibrium concentration) was determined according to the procedure established by the American Society for Testing and Material (ASTM) [58]. It is used to characterize the adsorbent performance and measure the activity level. The iodine number was estimated to be 434.62. A higher value of iodine number indicates a higher degree of activation [59]. After adsorption, there were no significant changes observed in the surface area and pore volume of the adsorbent. This may be due to desorption of dye molecules on the adsorbent surface during regeneration of the adsorbent. While determining surface area, the regeneration temperature was maintained at 353 K. A similar observation has been reported elsewhere [60]. The physical characteristics of the GLP were determined, and results are summarized in Table S1 of supplementary materials. It shows that the lower % of moisture and ash content signifies better quality of the adsorbent [61]. The initial and final ATR spectra of the GLP after RBBR adsorption are shown in Figs. 3a and b, respectively. The ATR spectrum of the GLP adsorbent before adsorption shows a broad and strong peak at 3,296.34 $cm^{-1}$, representing the O–H stretching vibration of bonded hydroxyl groups. The short peak observed at 2,873.93 $cm^{-1}$ was due to the C–H bending vibrations of methyl groups. The peak observed at 2,304.9 $cm^{-1}$ was due to O=C=O stretching of alkyne group. The wave number observed at 1,041.5 $cm^{-1}$ was assigned to the C–O stretching vibration of carboxylic acid and alcoholic groups. The absorption band at the frequency of 1,932.52 $cm^{-1}$ is assigned to C=O stretching vibration in carboxylic anhydrides. Similarly, the presence of C=O stretching vibrations of carbonyl groups of carboxylic acid, aromatic aldehyde and ketones with intermolecular hydrogen bond was observed from the peak at 1,620.2 $cm^{-1}$. After adsorption, the significant changes have been observed in band intensities of hydroxyl (3,296.34 $cm^{-1}$), methyl (2,873.93 $cm^{-1}$), and carbonyl (1,620.2 $cm^{-1}$) groups in the ATR spectra of RBBR dye loaded with GLP adsorbent (Fig. 3b). Thus, the ATR analysis demonstrated that more hydroxyl, methyl, and carbonyl groups were present on the surface of the adsorbent. These groups may act as possible binding sites for electrostatic interactions with the anionic dye molecules [28,44,62]. SEM images of the GLP before and after adsorption of RBBR dye are shown in Figs. 4a and b. As seen from Fig. 4a, adsorbent has an irregular, rough and porous surface. The rough surfaces are favorable for the adsorption of dye molecules onto the adsorbent [60]. The presence of dye molecules loaded onto the surface and pores of the adsorbent after adsorption are shown in Fig. 4b. Analytical SEM at 20 keV equipped with EDS was used to determine the elemental composition of the adsorbent. The chemical characteristics of the surface of the GLP adsorbent are given in Table S2. It shows that the adsorbent surface mainly contains the elements of carbon and oxygen. After adsorption the weight % of elemental carbon and oxygen increases, suggesting that the particle surface is loaded with dye anions.

### 3.2. Analysis of batch adsorption studies

#### 3.2.1. Effect of initial pH

The process of adsorption between the adsorbent surface and the adsorbate solution is highly dependent on the pH value of the medium and the zero-point charge ($pH_{pzc}$) of

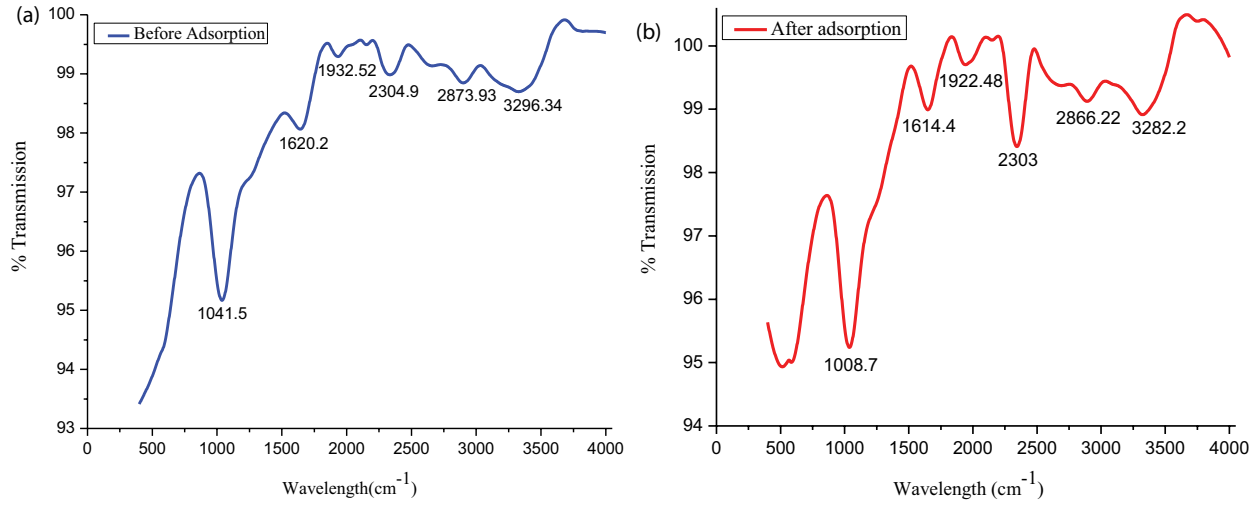


Fig. 3. (a) ATR spectrum of GLP adsorbent before RBBR dye adsorption. (b) ATR spectrum of GLP adsorbent after RBBR dye adsorption.

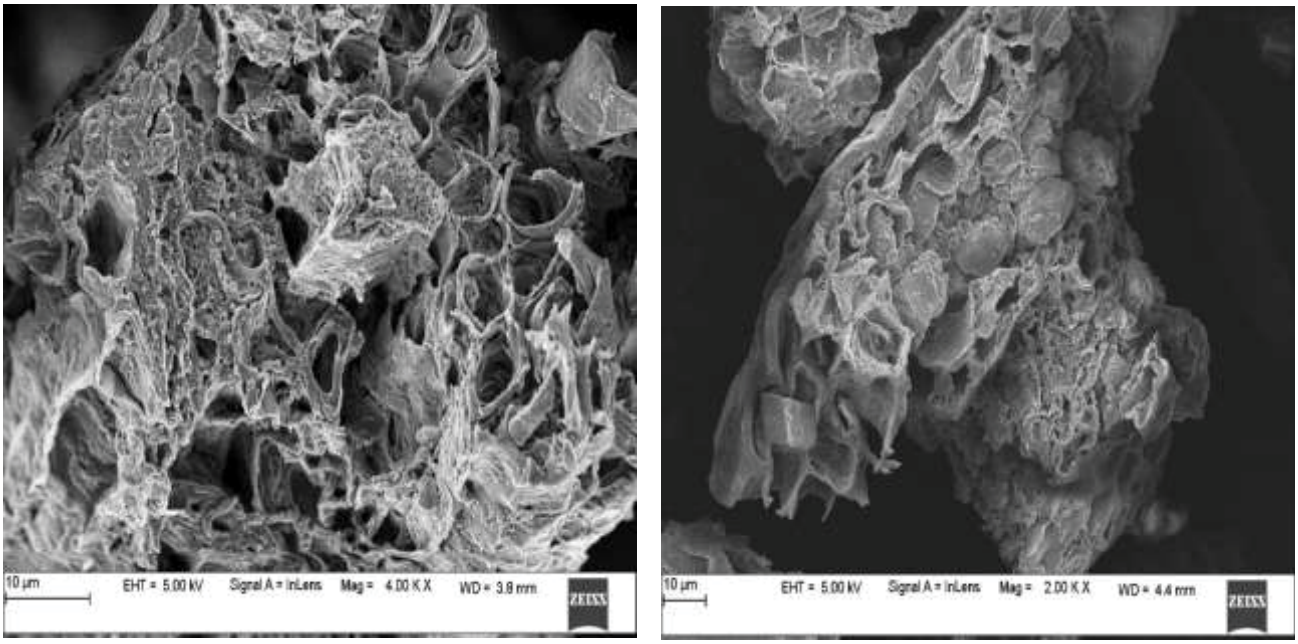


(a) (b)

Fig. 4. SEM micrograph of (a) GLP adsorbent before RBBR dye adsorption and (b) GLP adsorbent after RBBR dye adsorption.

the adsorbent. The pH point of zero charge of the adsorbent was determined by powder addition method [25]. The ΔpH values ($pH_{initial}$–$pH_{final}$) for the GLP adsorbent are plotted against the initial pH values (Fig. 5). The initial pH at which ΔpH becomes 0 is called $pH_{pzc}$. The zero-point charge of the GLP adsorbent was found to be at 6.5. The presence of $H^+$ and $OH^-$ ions in solution may change the potential surface charges of the adsorbent. If the pH of the solution is below the $pH_{zpc}$, the binding sites on the surface will be protonated (positively charged) by the presence of excess $H^+$ ions. If it is above its $pH_{zpc}$, the active sites on the surface will be deprotonated (negatively charged) by the $OH^-$ ions present in the solution. Anion adsorption on any adsorbent will be favorable at pH < $pH_{zpc}$. The effect of initial pH on adsorption of RBBR onto GLP adsorbent was analyzed by varying the pH of the dye solution from 2 to 10. Fig. S1 shows that the % dye removal was maximum at pH 2 (99.44%). At pH 2, a substantial electrostatic interaction (van der Waals forces) exists between the protonated binding sites of the adsorbent and anionic dye molecules. The elimination of this dye is favorable in the acidic medium than in the basic medium. After the pH was raised from 2 to 10, the decolorization efficiency dropped from 99.44% to 18.64%. The decrease in RBBR dye adsorption at basic pH is hypothesized to be due to the electrostatic repulsion between the negatively charged surface and the deprotonated RBBR. Since the pH of this solution increases, the active sites on the surface of the adsorbent are going to be deprotonated by the existence of extra $OH^-$ ions, thus the amount of negatively-charged sites rises. Further, decreased adsorption of RBBR found at basic pH might be a result of rivalry between the surplus hydroxyl ions as well as the negatively charged dye ions for the adsorption binding sites [3].

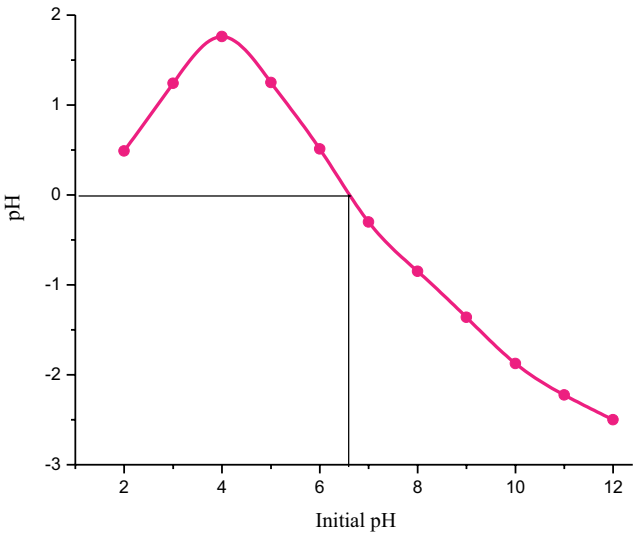


Fig. 5. Zero-point charge ($pH_{zpc}$) plot of GLP adsorbent (sodium chloride concentration: 0.1 M; adsorbent dosage: 10 g $L^{-1}$; adsorbent particle size: 105 µm; agitation speed: 150 rpm: temperature: 303 K; contact time 24 h).

### 3.2.2. Effect of adsorbent dosage

Adsorbent dosage is another important parameter for the determination of the adsorption capacity. The removal of dye with varying amount of adsorbent from 1 to 9 g $L^{-1}$ was studied for fixed initial dye concentration of 100 mg $L^{-1}$ at pH 2. From Fig. 6 it can be seen that the decolorization efficiency of RBBR increased from 75.51% to 99.25%, but

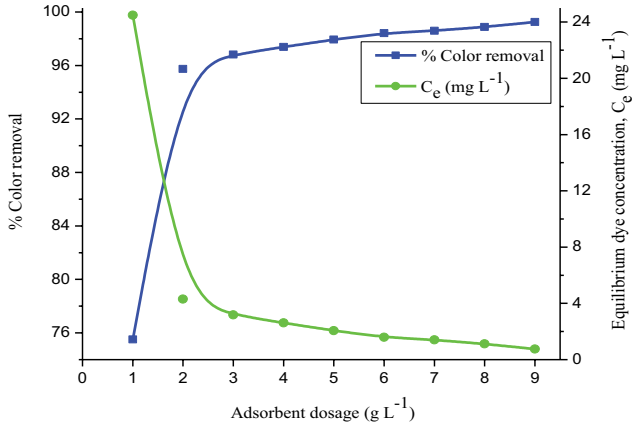


Fig. 6. Effect of GLP adsorbent dosage on RBBR dye adsorption (initial pH: 2; initial dye concentration: 100 mg $L^{-1}$; adsorbent particle size: 105 μm; agitation speed: 150 rpm; temperature: 303 K; contact time: 24 h).

the equilibrium dye concentration in the solution ($C_e$) gets decreased from 24.49 to 0.475 mg $L^{-1}$ with the increase in the adsorbent dosage from 1 to 9 g $L^{-1}$. The % color removal of dye increased by 27% when the quantity of GLP used was doubled from 1 to 2 g $L^{-1}$. The increase in the decolorization efficiency with the adsorbent dosage can be attributed to the availability of greater surface area resulted in the increase in the availability of adsorption active sites [63]. In other words, at higher adsorbent-to-dye concentration ratios, adsorption on the particle surface is very rapid, thus producing a lower adsorbate concentration in the solution, compared with that obtained for a lesser adsorbent-to-dye concentration ratio. But when the equilibrium adsorption capability is expressed in milligrams dye adsorbed per gram of the adsorbent at equilibrium ($q_e$), the capacity decreases when the quantity of adsorbent raises [64] (figure not shown). This is mainly due to the split in the flux or concentration gradient between the dye concentration in the solution and that at the surface of the adsorbent. Hence the competition for the availability of active sites for the adsorption of dye declines with the increase in the adsorbent dose [55]. This implies that as the amount of particles increases, there might be many adsorbent particles in solution, which might cause overlapping of adsorption binding sites or adsorbed species causing the particles to aggregate, thereby resulting in reduced adsorption active sites per unit mass of the adsorbent [65]. At high adsorbent dosage, due to agglomeration of adsorbent particles there is a decrease in overall active surface area of the adsorbent and a rise in diffusion path length and hence, the adsorption capacity decreases [66].

#### 3.2.3. Effect of adsorbent particle size

The effect of particle size on adsorption of RBBR onto GLP is shown in Fig. S2. The % color removal of dye is proportional to surface area available for adsorption. Since the surface areas increases with decrease in particle size, there will be more adsorption when smaller size particles are used. The results show that the decolorization of RBBR decreased gradually from 95.80% to 65.24% with an increase in adsorbent particle size from 72 to 538 μm. This relationship indicates that powdered adsorbent would be advantageous over granular particles. Also, the smaller particles will have a shorter diffusion path, thus allowing the adsorbate molecules to pierce deeper into the solid particle rapidly, resulting in a higher % adsorption [67].

#### 3.2.4. Effect of agitation speed

The effect of agitation speed in a batch adsorption process is essential to overcome the external diffusion resistance. Effect of agitation speed on color removal was evaluated by varying the agitation speed from 0 to 200 rpm at 303 K. Fig. S3 shows that the % color removal increased from 43.65% to 97.28% with increasing agitation speed. The increase in removal efficiency may be due to increase in turbulence attributable to reducing the thickness of film resistance surrounding the particles of guava leaf adsorbent, thus increasing external film diffusion and uptake of RBBR dye molecules [68]. This phenomenon may be explained by increasing the contact surface of adsorbent–dye solution and favoring the transfer of dye molecules to the binding sites of the adsorbent.

### 3.3. Analysis of factorial experimental design and optimization of process parameters

The important factors for adsorption of RBBR onto GLP adsorbent were initial values of pH, adsorbent dosage, dye concentration and adsorbent particle size. The comparison of predicted response values with 31 sets of batch adsorption experimental results is reported in Table 2. The results for % color removal and equilibrium dye uptake ($q_e$) were analyzed by analysis of variance (ANOVA) and are given in Tables 3 and 4, respectively. The probability level, $P$ indicates the significance of each of the interactions among the independent variables and Student $T$-tests were applied to evaluate the importance of the regression coefficient of the process factors. Larger values of $T_{statistics}$ and lower values of $p$ ($p < 0.05$) for linear, square, and interaction effects are more significant in the chosen model at the corresponding coefficient terms. From Table 3, the coefficients for the linear effect of initial dye concentration ($X_2$), adsorbent dosage ($X_3$) and particle size ($X_4$) were the first important factors ($p = 0.000$). The coefficient for the linear effect of initial pH ($X_1$) did not signify the effect on color removal ($p = 0.082$). The coefficients of the quadratic effect of $X_3$ and $X_2$ were the first and second important factors ($p = 0.007$, $p = 0.038$), respectively. The coefficients of the quadratic effect of the variables $X_1$ and $X_4$ are not significant. The coefficient of the interaction effect of $X_1X_4$ was found to be significant ($p = 0.001$). However, the coefficients of the other interactive effects ($X_1X_2$, $X_1X_3$, $X_2X_3$, $X_2X_4$, $X_3X_4$) among the variables did not appear to be significant. A larger value of $F_{statistics}$ indicates that most of the variation in the response can be explained by the regression model equation [69]. The regression model Eq. (28) for % RBBR dye removal is

$$\%\ \text{RBBR dye removal} = 84.91 - 0.8667\,X_1 - 5.0625\,X_2 + 4.78\,X_3 - 2.9708\,X_4 + 0.1059\,X_1^2 - 0.9677\,X_2^2 - 1.3265\,X_3^2 + 0.3672\,X_4^2 - 1.1587\,X_1X_2 + 0.3687\,X_1X_3 + 2.2612\,X_1X_4 + 0.2012\,X_2X_3 + 0.6862\,X_2X_4 - 0.8312\,X_3X_4 \quad (28)$$

Table 2
Batch adsorption experiments as per CCD matrix for RBBR dye removal by GLP adsorbent

| Run no. | $X_1$ | $X_2$ (mg $L^{-1}$) | $X_3$ (g $L^{-1}$) | $X_4$ (μm) | % RBBR color removal | | Equilibrium dye uptake $q_e$ (mg $g^{-1}$) | |
|---|---|---|---|---|---|---|---|---|
| | | | | | Experiment | Predicted | Experiment | Predicted |
| 1 | –1 | –1 | 1 | 1 | 85.29 | 85.32 | 51.17 | 49.37 |
| 2 | 0 | 0 | 0 | 0 | 84.86 | 84.91 | 84.86 | 84.91 |
| 3 | 1 | –1 | –1 | –1 | 82.86 | 84.06 | 82.86 | 84.82 |
| 4 | 2 | 0 | 0 | 0 | 80.34 | 83.60 | 80.34 | 83.08 |
| 5 | 1 | –1 | 1 | 1 | 89.46 | 91.16 | 53.67 | 56.08 |
| 6 | 0 | –2 | 0 | 0 | 92.25 | 91.16 | 46.12 | 42.83 |
| 7 | 0 | 0 | 0 | 0 | 84.9 | 84.91 | 84.90 | 84.91 |
| 8 | –1 | –1 | –1 | –1 | 90.34 | 88.74 | 90.34 | 90.53 |
| 9 | 0 | 0 | 0 | 0 | 84.82 | 84.91 | 84.82 | 84.91 |
| 10 | 0 | 0 | 0 | 2 | 79.65 | 80.44 | 79.65 | 80.74 |
| 11 | –1 | 1 | –1 | –1 | 80.65 | 79.15 | 134.42 | 131.70 |
| 12 | 0 | 0 | –2 | 0 | 67.12 | 70.04 | 134.24 | 133.79 |
| 13 | 0 | 0 | 0 | –2 | 90.74 | 92.32 | 90.74 | 92.16 |
| 14 | –1 | 1 | 1 | –1 | 89 | 90.04 | 89.00 | 88.97 |
| 15 | 0 | 2 | 0 | 0 | 67.46 | 70.91 | 101.19 | 106.99 |
| 16 | 0 | 0 | 0 | 0 | 85.02 | 84.91 | 85.02 | 84.91 |
| 17 | –1 | –1 | –1 | 1 | 76.38 | 78.56 | 76.38 | 80.15 |
| 18 | 1 | 1 | –1 | –1 | 72.44 | 69.84 | 120.73 | 120.33 |
| 19 | 0 | 0 | 0 | 0 | 84.94 | 84.91 | 84.94 | 84.91 |
| 20 | 0 | 0 | 0 | 0 | 84.9 | 84.91 | 84.90 | 84.91 |
| 21 | 1 | 1 | 1 | –1 | 84.18 | 82.20 | 84.18 | 80.10 |
| 22 | 0 | 0 | 0 | 0 | 84.92 | 84.91 | 84.92 | 84.91 |
| 23 | –1 | 1 | 1 | 1 | 80.28 | 79.29 | 80.28 | 78.01 |
| 24 | –1 | 1 | –1 | 1 | 72.83 | 71.72 | 121.38 | 120.82 |
| 25 | –1 | –1 | 1 | –1 | 97.44 | 98.82 | 58.46 | 59.83 |
| 26 | –2 | 0 | 0 | 0 | 87.96 | 87.07 | 87.96 | 87.73 |
| 27 | 1 | –1 | 1 | –1 | 97.08 | 95.62 | 58.25 | 56.61 |
| 28 | 1 | 1 | 1 | 1 | 81.46 | 80.50 | 81.46 | 79.07 |
| 29 | 1 | –1 | –1 | 1 | 86.54 | 82.93 | 86.54 | 84.37 |
| 30 | 0 | 0 | 2 | 0 | 89.72 | 89.16 | 59.81 | 62.77 |
| 31 | 1 | 1 | –1 | 1 | 72.63 | 71.46 | 121.05 | 119.38 |

From Table 4, the coefficients for the linear effect of initial dye concentration ($X_2$), adsorbent dosage ($X_3$) and particle size ($X_4$) were the first important factors ($p = 0.000$). The coefficient for the linear effect of initial pH ($X_1$) did not signify the effect on adsorption capacity at equilibrium ($p = 0.071$). The coefficients of the quadratic effect of $X_2$ and $X_3$ were the first important factors ($p = 0.000$). The coefficients of the quadratic effect of the variables $X_1$ and $X_4$ are not significant. The coefficients of the interaction effects of $X_2X_3$ and $X_1X_4$ were the first and second most important factors ($p = 0.001$, 0.004). However, the coefficients of the other interactive effects ($X_1X_2$, $X_1X_3$, $X_2X_4$, $X_3X_4$) among the variables did not appear to be significant. The regression model Eq. (29) for equilibrium dye uptake is

$$\text{RBBR dye uptake at equilibrium} = 84.91 - 1.1637X_1 + 16.0404X_2 - 17.7537X_3 - 2.8537X_4 + 0.1236X_1^2 - 2.5X_2^2 + 3.3423X_3^2 + 0.3848X_4^2 - 1.4144X_1X_2 + 0.6244X_1X_3 + 2.4818X_1X_4 - 3X_2X_3 - 0.1256X_2X_4 - 0.0194X_3X_4 \quad (29)$$

The suitability of the response surface model was assessed by the values of regression coefficient ($R^2$), coefficient of variation, adequate precision and by the analysis of lack of fit.

The regression coefficient, $R^2$, indicates the goodness of fit of experimental data and the predicted responses with negligible error. The predicted values of % color removal and equilibrium dye uptake match the experimental values reasonably well with $R^2$ of 0.9503 and 0.9907, respectively. It indicates that more than 95% of the variations in response could be described by the above model equations (Eqs. (28) and (29)). It also means that the model does not explain less than 5% of the variation. The adjusted $R^2$ is a tool to measure the excellence of fitting, but it is more appropriate for comparing models with various process parameters. It rectifies the $R^2$ value for the number of terms in the model and the sample size by using the degrees of freedom in its computations. Predicted $R^2$ can prevent overfitting the model and can be calculated from predicted residual sum of squares

Table 3
ANOVA for % color removal of RBBR dye using GLP adsorbent from the data of CCD experiments

| Term | Coefficient | SE of coefficient | $T_{statistics}$ | DF | Seq SS | Adj SS | Adj MS | $F_{statistics}$ | Probability |
|---|---|---|---|---|---|---|---|---|---|
| Constant | 84.9086 | 0.8647 | 98.190 | | | | | | 0.000 |
| Regression | | | | 14 | 1,600.41 | 1,600.41 | 114.315 | 21.84 | 0.000 |
| Linear | | | | 4 | 1,393.30 | 1,393.30 | 348.326 | 66.55 | 0.000 |
| $X_1$ | –0.8667 | 0.4670 | –1.856 | 1 | 18.03 | 18.03 | 18.027 | 3.44 | 0.082 |
| $X_2$ (mg $L^{-1}$) | –5.0625 | 0.4670 | –10.840 | 1 | 615.09 | 615.09 | 615.094 | 117.51 | 0.000 |
| $X_3$ (g $L^{-1}$) | 4.7800 | 0.4670 | 10.235 | 1 | 548.36 | 548.36 | 548.362 | 104.76 | 0.000 |
| $X_4$ (μm) | –2.9708 | 0.4670 | –6.361 | 1 | 211.82 | 211.82 | 211.820 | 40.47 | 0.000 |
| Square | | | | 4 | 82.40 | 82.40 | 20.599 | 3.94 | 0.021 |
| $X_1$ * $X_1$ | 0.1060 | 0.4278 | 0.248 | 1 | 2.23 | 0.32 | 0.321 | 0.06 | 0.808 |
| $X_2$ (mg $L^{-1}$) ×$X_2$ (mg $L^{-1}$) | –0.9678 | 0.4278 | –2.262 | 1 | 22.38 | 26.78 | 26.782 | 5.12 | 0.038 |
| $X_3$ (g $L^{-1}$) × $X_3$ (g $L^{-1}$) | –1.3265 | 0.4278 | –3.101 | 1 | 53.94 | 50.32 | 50.318 | 9.61 | 0.007 |
| $X_4$ (μm) × $X_4$ (μm) | 0.3672 | 0.4278 | 0.858 | 1 | 3.86 | 3.86 | 3.856 | 0.74 | 0.403 |
| Interaction | | | | 6 | 124.71 | 124.71 | 20.785 | 3.97 | 0.013 |
| $X_1$ × $X_2$ (mg $L^{-1}$) | –1.1587 | 0.5720 | –2.026 | 1 | 21.48 | 21.48 | 21.483 | 4.10 | 0.060 |
| $X_1$ × $X_3$ (g $L^{-1}$) | 0.3688 | 0.5720 | 0.645 | 1 | 2.18 | 2.18 | 2.176 | 0.42 | 0.528 |
| $X_1$ × $X_4$ (μm) | 2.2612 | 0.5720 | 3.953 | 1 | 81.81 | 81.81 | 81.812 | 15.63 | 0.001 |
| $X_2$ (mg $L^{-1}$) × $X_3$ (g $L^{-1}$) | 0.2013 | 0.5720 | 0.352 | 1 | 0.65 | 0.65 | 0.648 | 0.12 | 0.730 |
| $X_2$ (mg $L^{-1}$) × $X_4$ (μm) | 0.6862 | 0.5720 | 1.200 | 1 | 7.54 | 7.54 | 7.535 | 1.44 | 0.248 |
| $X_3$ (g $L^{-1}$) × $X_4$ (μm) | –0.8312 | 0.5720 | –1.453 | 1 | 11.06 | 11.06 | 11.056 | 2.11 | 0.165 |
| Residual error | | | | 16 | 83.75 | 83.75 | 5.234 | | |
| Lack-of-fit | | | | 10 | 83.73 | 83.73 | 8.373 | 2103.16 | 0.000 |
| Pure error | | | | 6 | 0.02 | 0.02 | 0.004 | | |
| Total | | | | 30 | 1,684.16 | | | | |

Regression coefficient, $R^2$ = 95.03%, $R^2$ (Pred) = 71.36%, $R^2$ (adj) = 90.68%, $S$ = 2.28787, PRESS = 482.294.

(PRESS) statistics. A greater value of predicted $R^2$ indicates the models of more predictive potential. This may indicate that an over fitted model will not predict any new observations nearly as well as it fits the existing data. The term PRESS statistics is used to forecast the responses of another experiment and the lesser value of PRESS is more perfect [32]. A lower value of RMSE (1.643 for color removal; 2.115 for equilibrium dye uptake) and AAD (1.583% for color removal; 2.036% for equilibrium dye uptake) yields the best fit model equation. The adequacy of the model was evaluated by the residual error which measures the error between observed and the predicted response values. The repetition of central points was used to obtain the standard error of the coefficients. The ANOVA Tables 3 and 4 shows the residual error, which measures the elements of variation in the response that cannot be explained by the model, and their occurrence in a normal distribution (Fig. not shown).

### *3.3.1. Contour and response surface plots*

Contour and response surface plots were used to study the mutual interactions among the variables and to measure the maximum response level of each variable. The coordinates of the central point in each of these contour plot indicate the optimal value of the respective constituents. The central point is the point at which the slope of the contour is zero in all directions. The maximum predicted value of response variable shown by the minimum curvature of the contour plot. The contour plots for % color removal of RBBR are shown in Figs. 7a and b. Fig. 7a shows that the contour plot of % color removal from the aqueous solution as a function of initial pH and dye concentration. It occurs when the initial dye concentration ranges between 100 and 150 mg $L^{-1}$, pH in the range of 1.85–2.4, and the effect is insignificant. Fig. 7b shows that the maximum decolorization efficiency occurs when the adsorbent dosage ranges between 2.25 and 3 g $L^{-1}$ and the particle size ranges from 105 to 120 μm. The contour plots for equilibrium dye uptake are shown in Figs. 8a and b. Fig. 8a shows that the maximum adsorption capacity occurs when the pH ranges between 1.6 and 2.3, and the adsorbent dosage in the range of 1–1.25 g $L^{-1}$. Fig. 8b shows that the highest predicted adsorption capacity occurs when the initial dye concentration ranges between 225 and 300 mg $L^{-1}$ and the adsorbent particle size ranges from 105 to 185 μm, and the effect is not very significant. Response surface plots are derived as a function of two factors while keeping all other factors at fixed levels. The optimum situations of the relative variables will resemble the coordinates of the central point in the upmost level in each of these figures. The response surface curves for % color removal of RBBR are shown in Figs. 9a and b. Fig. 9a shows the surface plot of the response variable as a function of initial pH and initial dye

Table 4
ANOVA for response surface quadratic model for equilibrium dye uptake of RBBR using GLP adsorbent

| Term | Coefficient | SE of coefficient | $T_{statistics}$ | DF | Seq SS | Adj SS | Adj MS | $F_{statistics}$ | Probability |
|---|---|---|---|---|---|---|---|---|---|
| Constant | 84.9086 | 1.1130 | 76.290 | | | | | | 0.000 |
| Regression | | | | 14 | 14,807.4 | 14,807.4 | 1,057.67 | 121.98 | 0.000 |
| Linear | | | | 4 | 13,967.7 | 13,967.7 | 3,491.93 | 402.72 | 0.000 |
| $X_1$ | –1.1637 | 0.6011 | –1.936 | 1 | 32.5 | 32.5 | 32.50 | 3.75 | 0.071 |
| $X_2$ (mg $L^{-1}$) | 16.0404 | 0.6011 | 26.686 | 1 | 6,175.1 | 6,175.1 | 6,175.08 | 712.16 | 0.000 |
| $X_3$ (g $L^{-1}$) | –17.7537 | 0.6011 | –29.537 | 1 | 7,564.7 | 7,564.7 | 7,564.70 | 872.42 | 0.000 |
| $X_4$ (μm) | –2.8537 | 0.6011 | –4.748 | 1 | 195.5 | 195.5 | 195.45 | 22.54 | 0.000 |
| Square | | | | 4 | 558.0 | 558.0 | 139.51 | 16.09 | 0.000 |
| $X_1 \times X_1$ | 0.1236 | 0.5507 | 0.224 | 1 | 0.0 | 0.4 | 0.44 | 0.05 | 0.825 |
| $X_2$ (mg $L^{-1}$) × $X_2$ (mg $L^{-1}$) | –2.5002 | 0.5507 | –4.540 | 1 | 238.5 | 178.7 | 178.75 | 20.61 | 0.000 |
| $X_3$ (g $L^{-1}$) × $X_3$ (g $L^{-1}$) | 3.3423 | 0.5507 | 6.070 | 1 | 315.2 | 319.4 | 319.45 | 36.84 | 0.000 |
| $X_4$ (μm) × $X_4$ (μm) | 0.3848 | 0.5507 | 0.699 | 1 | 4.2 | 4.2 | 4.24 | 0.49 | 0.495 |
| Interaction | | | | 6 | 281.6 | 281.6 | 46.93 | 5.41 | 0.003 |
| $X_1 \times X_2$ (mg $L^{-1}$) | –1.4144 | 0.7362 | –1.921 | 1 | 32.0 | 32.0 | 32.01 | 3.69 | 0.073 |
| $X_1 \times X_3$ (g $L^{-1}$) | 0.6244 | 0.7362 | 0.848 | 1 | 6.2 | 6.2 | 6.24 | 0.72 | 0.409 |
| $X_1 \times X_4$ (μm) | 2.4819 | 0.7362 | 3.371 | 1 | 98.6 | 98.6 | 98.56 | 11.37 | 0.004 |
| $X_2$ (mg $L^{-1}$) × $X_3$ (g $L^{-1}$) | –3.0056 | 0.7362 | –4.083 | 1 | 144.5 | 144.5 | 144.54 | 16.67 | 0.001 |
| $X_2$ (mg $L^{-1}$) × $X_4$ (μm) | –0.1256 | 0.7362 | –0.171 | 1 | 0.3 | 0.3 | 0.25 | 0.03 | 0.867 |
| $X_3$ (g $L^{-1}$) × $X_4$ (μm) | –0.0194 | 0.7362 | –0.026 | 1 | 0.0 | 0.0 | 0.01 | 0.00 | 0.979 |
| Residual error | | | | 16 | 138.7 | 138.7 | 8.67 | | |
| Lack-of-fit | | | | 10 | 138.7 | 138.7 | 13.87 | 3,484.36 | 0.000 |
| Pure error | | | | 6 | 0.0 | 0.0 | 0.00 | | |
| Total | | | | 30 | 14,946.1 | | | | |

Regression coefficient, $R^2$ = 99.07%, $R^2$ (Pred) = 94.65%, $R^2$ (adj) = 98.26%, $S$ = 2.94464, PRESS = 799.006.
where SE, standard error of coefficient; DF, degree of freedom; Seq SS, sequential sum of squares; Adj SS, adjusted sum of squares; Adj MS, adjusted mean squares; PRESS, predicted residual sum of squares; $S$, value of $S$ chart.

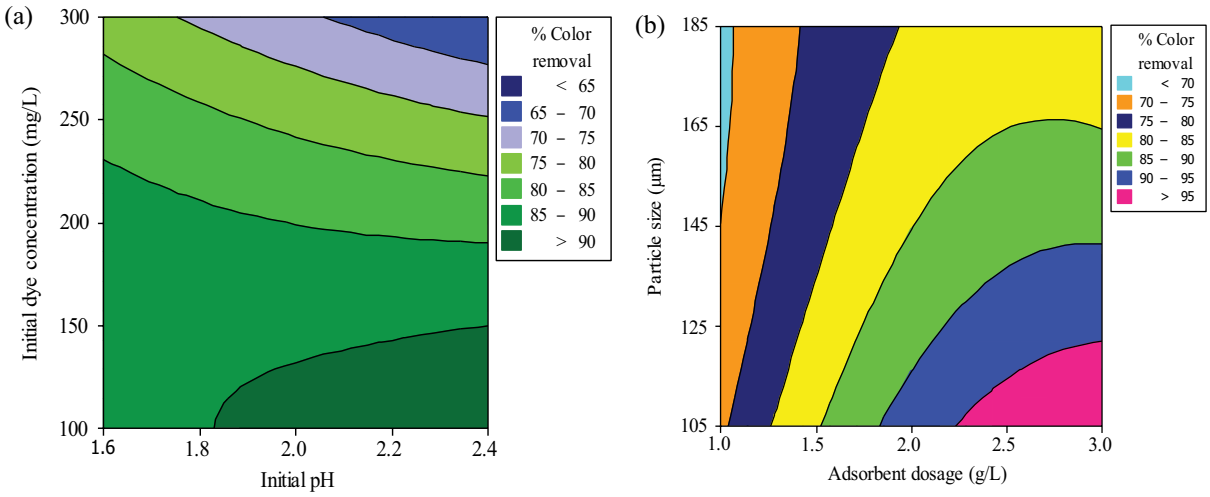


Fig. 7. Contour plots for interactive effect of (a) initial dye concentration and pH and (b) particle size and adsorbent dosage on color removal of RBBR dye.

concentration. It clearly shows that the % color removal of RBBR increases with decrease in the pH and initial dye concentration. For pH range of 1.6–2.4 and the dye concentration in the range of 100–300 mg $L^{-1}$ shows a significant effect on color removal from aqueous solution. Fig. 9b shows that with an increase in the amount of adsorbent and decrease in particle size, the % color removal improves. The response plot of adsorbent dosage in the ranges between 1 and 3 g $L^{-1}$

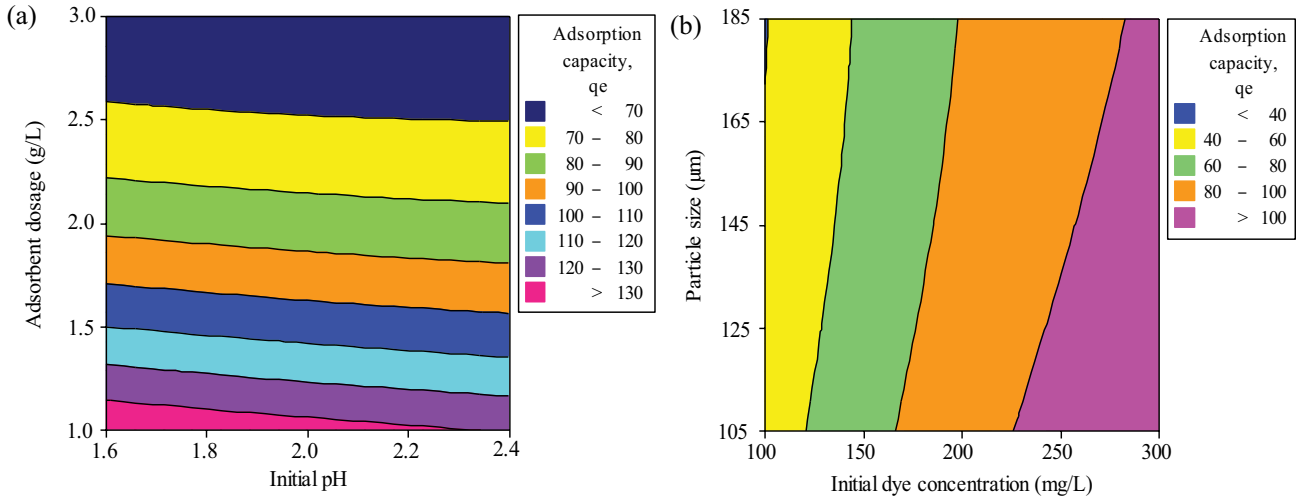


Fig. 8. Contour plots for interactive effect of (a) adsorbent dosage and initial pH, and (b) particle size and initial dye concentration on equilibrium dye uptake of RBBR.

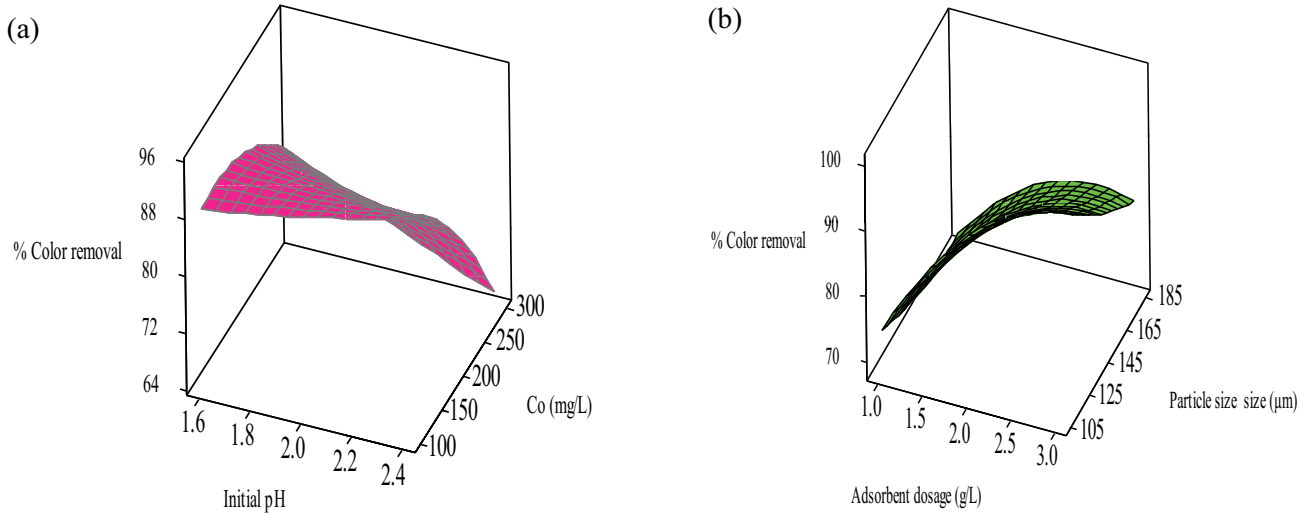


Fig. 9. Response surface plots for interactive effect of (a) initial dye concentration and pH and (b) particle size and adsorbent dosage on color removal of RBBR dye.

vs. particle size in the range of 105–185 µm shows a significant effect on decolorization. The response surface plots for equilibrium dye uptake of RBBR are shown in Figs. 10a and b. Fig. 10a suggests that the dye adsorption capacity at equilibrium decreases with an increase in adsorbent dosage and increase in pH. The response plot of adsorbent dosage ranges between 1 and 3 g $L^{-1}$ vs. the initial pH of dye solution in the range of 1.6–2.4 shows a significant effect on equilibrium dye uptake. Similarly, Fig. 10b shows that with an increase in the dye concentration and decrease in the adsorbent particle size, the adsorption capacity improves. The response surface plot of dye concentration in the range of 100–300 mg $L^{-1}$ vs. the adsorbent particle size in the ranges between 105 and 185 µm shows a significant effect on the uptake of RBBR from aqueous solution. The calculated values of response variables acquired from the regression model equations are closely related with those values found from the experiment and response surface plots under optimum conditions. A similar observation has been reported in another study by Vairavel and Murty [30].

### 3.3.2. Process model validation

Three solutions with different values of ideal initial conditions were used to forecast the best conditions for RBBR dye adsorption by GLP adsorbent which is shown in Tables 5 and 6. Different experiments were done under various levels of the factors and the results were matched to the predicted responses. From Table 5, the maximum color removal efficiency (97.44%) was obtained in the experiment number 3 compared with the other two experiments. From Table 6, the maximum equilibrium adsorption capacity (134.42 mg $g^{-1}$) was obtained in the experiment number 1 compared with the other two experiments. The optimal values of the process

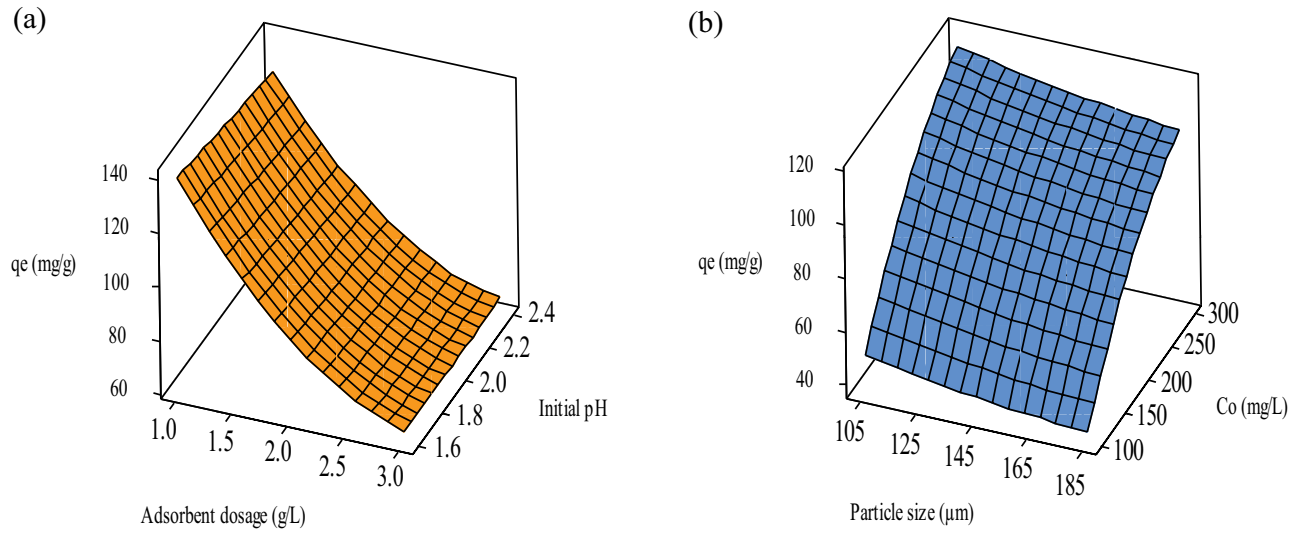


Fig. 10. Response surface plots for interactive effect of (a) initial pH and adsorbent dosage and (b) initial dye concentration and particle size on equilibrium dye uptake of RBBR.

Table 5
Validation of process model for RBBR dye adsorption

| Expt. | Process parameters with operating conditions | | | | RBBR decolorization efficiency (%) | |
|---|---|---|---|---|---|---|
| | $X_1$ | $X_2$ (mg $L^{-1}$) | $X_3$ (g $L^{-1}$) | $X_4$ (μm) | Actual value | Predicted value |
| 1 | 1.8 | 150 | 2.5 | 125 | 97.44 | 98.26 |
| 2 | 2.0 | 200 | 2.0 | 145 | 85.02 | 86.34 |
| 3 | 1.8 | 150 | 1.5 | 165 | 76.38 | 76.92 |

Table 6
Validation of process model for equilibrium dye uptake of RBBR

| Expt. | Process parameters with operating conditions | | | | Equilibrium dye uptake $q_e$ (mg $g^{-1}$) | |
|---|---|---|---|---|---|---|
| | $X_1$ | $X_2$ (mg $L^{-1}$) | $X_3$ (g $L^{-1}$) | $X_4$ (μm) | Actual value | Predicted value |
| 1 | 1.8 | 250 | 1.5 | 125 | 134.42 | 136.18 |
| 2 | 2.0 | 300 | 2.0 | 145 | 101.19 | 102.94 |
| 3 | 1.8 | 150 | 1.5 | 125 | 90.34 | 90.85 |

independent variables for maximal response are given in Table 7. The comparison between experimental and predicted responses shows a good relation between them, and it indicates that the empirical models resulted from the design could as well be used for describing the relation between process independent variables and the response in RBBR dye decolorization. The optimization studies clearly revealed that the RSM was a good method to predict the ideal conditions for best decolorization efficiency and equilibrium adsorption capacity.

### 3.4. Inference from adsorption isotherm models

The linearized Langmuir, Freundlich, and Temkin isotherms plots for the adsorption of RBBR dye by the GLP adsorbent at 303 K are shown in Figs. 11, S4, and S5, respectively. The results of model parameters obtained from regressive analysis of these plots are presented in Table 8. It shows that the best fitted isotherm models were chosen in the order of prediction precision: Langmuir > Temkin > Freundlich isotherms. From Table 8, the higher value of the regression coefficient ($R^2$ = 0.9962) and lower value of chi-square ($\chi^2$ = 0.4229) were found in the Langmuir model, compared with the Temkin isotherm ($R^2$ = 0.9824, $\chi^2$ = 0.8045) and Freundlich ($R^2$ = 0.9448, $\chi^2$ = 3.3213) models. Hence the equilibrium adsorption data fitted very well with Langmuir isotherm model. According to the assumptions of the Langmuir isotherm, the adsorption was homogeneous in nature with the formation of monolayer at active sites [43]. The maximum adsorption capacity of the adsorbent ($q_{max}$) was estimated to be 93.12 mg $g^{-1}$. The calculated values of $R_L$ at different initial dye concentration are presented in Fig. S6. It shows that the

Table 7
Optimal values of the process independent variables for maximum decolorization efficiency and equilibrium dye uptake of RBBR

| Process parameters | Optimum value for color removal | RBBR color removal (%) | Optimum value for $q_e$ | Equilibrium dye uptake $q_e$ (mg g$^{-1}$) |
|---|---|---|---|---|
| $X_1$ | 1.8 | 97.44 | 1.8 | 134.42 |
| $X_2$ (mg L$^{-1}$) | 150 | | 250 | |
| $X_3$ (g L$^{-1}$) | 2.5 | | 1.5 | |
| $X_4$ (μm) | 125 | | 125 | |

Table 8
Adsorption isotherm model parameters for RBBR dye adsorption onto GLP adsorbent

| Isotherm | Model parameters | Values | Model equation |
|---|---|---|---|
| Freundlich | $n$ | 2.684 | $q_e = 25.087\ C_e^{0.3724}$ |
| | $K_F$ (L g$^{-1}$) | 25.087 | |
| | $R^2$ | 0.9448 | |
| | $\chi^2$ | 3.3213 | |
| Langmuir | $q_{max}$ (mg g$^{-1}$) | 93.124 | |
| | $K_L$ (L mg$^{-1}$) | 0.2674 | |
| | $R^2$ | 0.9962 | |
| | $\chi^2$ | 0.4279 | |
| Temkin | $K_T$ (L g$^{-1}$) | 3.8469 | $q_e = 17.262 \ln (3.8469\ C_e)$ |
| | $b_T$ (kJ mole$^{-1}$) | 0.1459 | |
| | $R^2$ | 0.9824 | |
| | $\chi^2$ | 0.8045 | |

adsorption was found to be more at higher initial dye concentrations. Also the $R_L$ (separation factor) values fell in the range of 0–1 at all initial dye concentration (50–250 mg L$^{-1}$) and this suggests that the adsorption process is favorable. At higher concentration, the adsorption process was found to be more favorable. The value of Freundlich constant, $n$ (2.684) is in-between 1 and 10 which again proved that the adsorption is favorable. The $q_{max}$ of the GLP adsorbent for the removal of RBBR was compared with those of other adsorbents from the literature are reported in Table 9. It can be inferred from the table that the prepared GLP adsorbent has superior adsorption capacity for the decolorization of RBBR dye on comparison with the reported adsorbents.

### *3.5. Inference from thermodynamic analysis for the adsorption of RBBR*

The results for equilibrium adsorption values ($q_e$) with various temperature and adsorbate concentrations are shown in Fig. 12. It can be seen that with the increase in temperature the equilibrium adsorption capacity increases. The maximum adsorption capacity, $q_{max}$ of RBBR dye molecules increased from 93.12 mg g$^{-1}$ at 303 K to 112.27 mg g$^{-1}$ at 323 K. The increase in decolorization efficiency, and equilibrium dye uptake onto the particle surface at higher temperature suggests that the adsorption process was rapid and endothermic in nature. This is because the pore volume of the GLP adsorbent particles was enlarged at elevated temperatures [20,29].

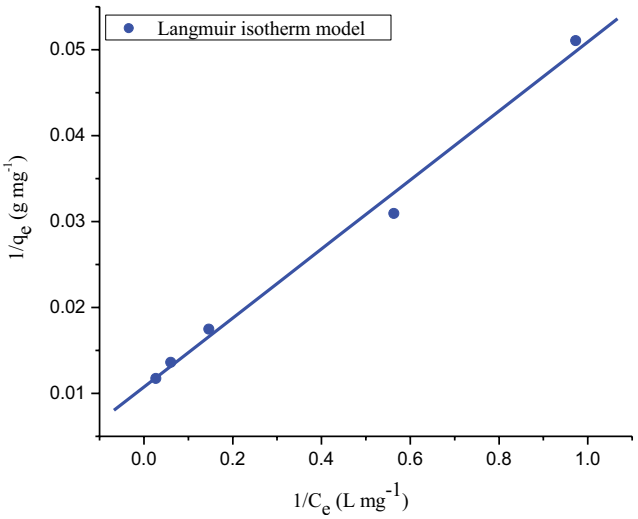


Fig. 11. Langmuir isotherm plot for adsorption of RBBR dye onto GLP adsorbent (initial pH: 1.8; initial dye concentration: 50–250 mg L$^{-1}$; adsorbent dosage: 2.5 g L$^{-1}$; particle size: 125 μm; agitation speed: 150 rpm; temperature: 303 K; contact time: 24 h).

The pore volume was observed to increase from 1.5 mm$^3$ g$^{-1}$ at room temperature (303 K) to 2.4 mm$^3$ g$^{-1}$ at 323 K. This phenomenon may be due to an increase in the diffusion of dye molecules across the boundary layer and the interior

Table 9
Comparison of maximum monolayer adsorption capacity of RBBR dye onto various adsorbents

| Adsorbent | Maximum adsorption capacity $q_{max}$ (mg $g^{-1}$) | References |
|---|---|---|
| Multi-walled carbon nano tubes | 6.89 | [11] |
| Pineapple leaf powder and lime leaf powder | 9.58 | [70] |
| Orange peel | 10.70 | [71] |
| Surfactant-modified zeolite | 13.90 | [72] |
| Bone char prepared by $CO_2$ atmosphere | 20.60 | [73] |
| Pirina pretreated with $HNO_3$ | 23.63 | [74] |
| Red mud | 27.80 | [75] |
| Polyaniline doped p-Toluene sulfonic acid | 28.27 | [76] |
| Zinc oxide | 38.90 | [5] |
| Polyaniline camphor sulfonic acid | 42.00 | [76] |
| Water hyacinth root powder | 58.82 | [77] |
| Activated carbon prepared from a pine cone | 60.98 | [78] |
| Macrophyte *Salvinia natans* | 61.90 | [79] |
| Immobilized *Scenedesmus quadricauda* (green algae) | 68.00 | [80] |
| Guava leaf powder | 93.12 | Present study |

structures of the solid leading to a reduction in the swelling of the adsorbate molecules with rising temperatures [17,29]. More of the dye particles can gain adequate energy to bind with the sites at the solid particle surface. The enhancement in the adsorption capacity at higher temperature suggests the chemical interaction between dye molecules and adsorbent or generation of some new adsorption binding sites in the particle surface [81]. In addition, at higher temperature may create a swelling effect within the inner structure of the adsorbent thus allowing more adsorbate molecules to diffuse additionally [30]. The thermodynamic parameters were calculated from the Van't Hoff plot (Fig. 13), and the values are reported in Table 10. It shows that the values of $\Delta G$ diminished with the increase in temperature, suggesting that the adsorption was a spontaneous process. The values of $\Delta G$ become more negative with raise in temperature, suggesting that higher temperatures promote the adsorption of dye molecules. A positive value of $\Delta H$ again proves that that the adsorption of RBBR onto the GLP adsorbent is an endothermic process. The positive value of $\Delta S$ suggests more chance of adsorbate molecules on the particle surface than in the dye solution. The activation energy ($E_a$) of adsorption was determined from the Arrhenius plot (Fig. 14) and found to be 67.26 kJ $mole^{-1}$ with an adsorbate concentration of 200 mg $L^{-1}$. The $E_a$ values are found in the ranges between 60.93 and 67.26 kJ $mole^{-1}$ at various adsorbate concentrations

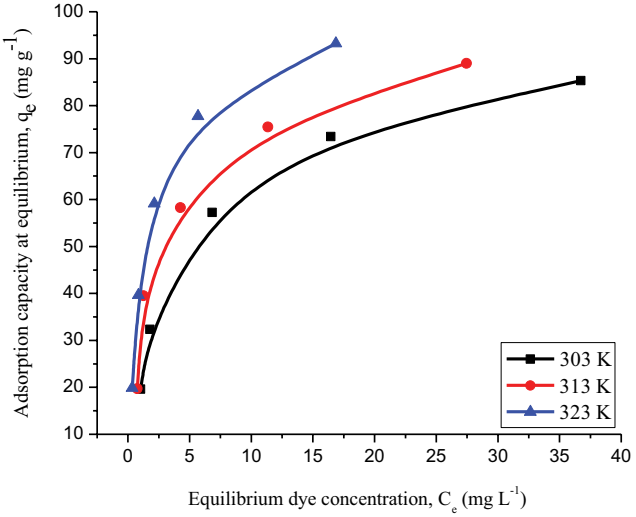


Fig. 12. Effect of temperature on adsorption of RBBR dye onto GLP adsorbent (initial pH: 1.8; initial dye concentration: 50–250 mg $L^{-1}$; adsorbent dosage: 2.5 g $L^{-1}$; particle size: 125 μm; agitation speed: 150 rpm; contact time: 24 h).

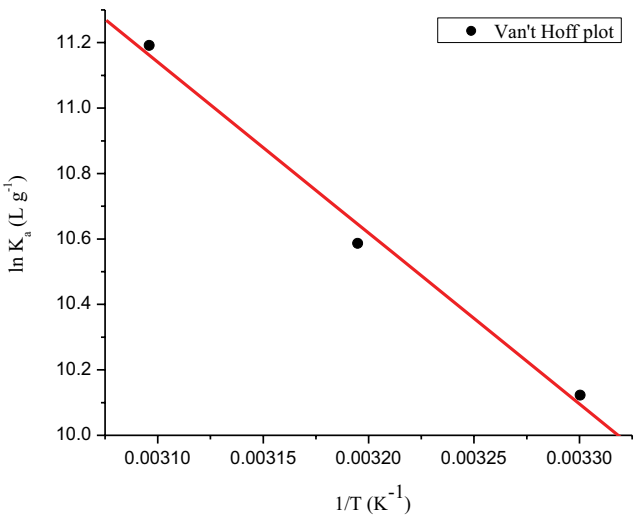


Fig. 13. Van't Hoff plot for adsorption of RBBR dye onto GLP adsorbent (initial pH: 1.8; initial dye concentration: 50–250 mg $L^{-1}$; adsorbent dosage: 2.5 g $L^{-1}$; particle size: 125 μm; agitation speed: 150 rpm; contact time: 24 h).

Table 10
Thermodynamic parameters for the adsorption of RBBR dye onto GLP adsorbent

| Temperature (K) | Maximum adsorption capacity $q_{max}$ (mg g$^{-1}$) | Thermodynamic parameters | | |
|---|---|---|---|---|
| | | $\Delta G$ (kJ mole$^{-1}$) | $\Delta H$ (kJ mole$^{-1}$) | $\Delta S$ (kJ mole$^{-1}$ K$^{-1}$) |
| 303 | 93.124 | –25.500 | | |
| 313 | 105.596 | –27.227 | 43.413 | 0.2272 |
| 323 | 112.271 | –30.054 | | |

and it is given in Table S3. The value of $\Delta H$ (43.413 kJ mole$^{-1}$) and activation energy (65.037 kJ mole$^{-1}$) indicates that dye adsorption onto the GLP adsorbent was chemisorptive process [42,45]. It may confirm that the covalent bond between RBBR dye molecules and binding sites on the solid particle at higher temperature [46].

### 3.6. Inference from adsorption kinetic models

The adsorption kinetics for the removal of RBBR onto the GLP adsorbent was rapid in the initial phases of the process. However, the dye uptake rate later diminished progressively with time. The active sites saturated at approximately 3 h for 50 mg L$^{-1}$, 4 h for 100 mg L$^{-1}$, 5 h for 150 mg L$^{-1}$, 6.5 h for 200 mg L$^{-1}$ and 8 h for 250 mg L$^{-1}$. Fig. S7 shows that the % color removal of RBBR slowly decreased from 97.94% to 85.31%, but the value of $q_e$ increased from 19.59 to 85.31 mg g$^{-1}$ with the increase in adsorbate concentration from 50 to 250 mg L$^{-1}$. The decrease in decolorization efficiency with rise in adsorbate concentration is due to aggregation of adsorbate in the active sites of the adsorbent (available binding sites on the adsorbent surface were saturated) and increased competition between the more adsorbate molecules at the fixed active sites of the adsorbent. Therefore, lack of available active sites in the adsorbent surface lead to decrease in the % adsorption [82]. The value of initial adsorption rate ($h$) enhanced from 10.594 to 17.458 mg g$^{-1}$ min$^{-1}$ with increase in initial adsorbate concentration. The greater in value of $q_e$ and $h$ is due to increase in concentration difference among the adsorbate concentration in the solution and the surface of the solid particle. This concentration gradient is the diffusion of adsorbate molecules from feed solution to the particle surface [83]. The linearized form of the pseudo-first-order and pseudo-second-order kinetic plots is shown in Figs. 15 and S8, respectively, and the results obtained from these plots were shown in Table 11. It was observed that the lower value of SD (0.29%–1.77%) and higher value of $R^2$ (0.9999) in the concentration ranges between 50 and 250 mg L$^{-1}$ suggests that the experimental data for decolorization of RBBR onto GLP adsorbent were appropriately fitted with pseudo-second-order model. Furthermore, the $q_e$ values evaluated from the pseudo-second-order model were closer to the experimental values at various adsorbate concentrations than that from the pseudo-first-order model. The predicted values of $q_e$ from pseudo-first-order kinetic model greatly diverged from the experimental values, higher value of SD and lower value of $R^2$ suggests that this model is not valid for adsorption of RBBR. It may be due to the existence of a boundary layer or to the mass transfer resistance from outer surface

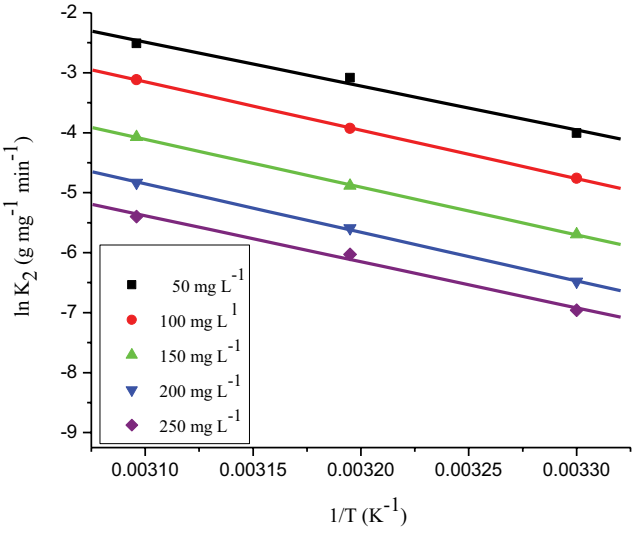


Fig. 14. Arrhenius plot for adsorption of RBBR dye onto GLP adsorbent (initial pH: 1.8; initial dye concentration: 50–250 mg L$^{-1}$; adsorbent dosage: 2.5 g L$^{-1}$; particle size: 125 μm; agitation speed: 150 rpm; contact time: 24 h).

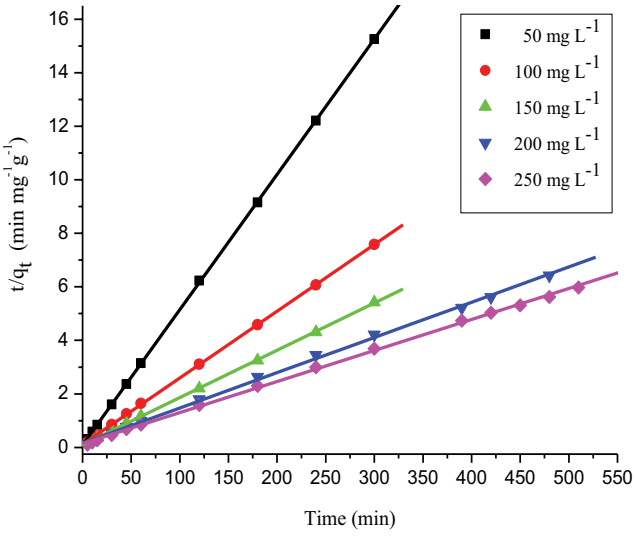


Fig. 15. Ho's pseudo-second-order kinetic plot for adsorption of RBBR dye onto GLP adsorbent (initial pH: 1.8; initial dye concentration: 50–250 mg L$^{-1}$; adsorbent dosage: 2.5 g L$^{-1}$; particle size: 125 μm; agitation speed: 150 rpm; contact time: 24 h).

Table 11
Kinetic parameters for the adsorption of RBBR dye onto GLP adsorbent

| Initial dye concentration (mg $L^{-1}$) | $q_{e,expt}$ (mg $g^{-1}$) | Pseudo-first-order kinetic model | | | | Pseudo-second-order kinetic model | | | | |
|---|---|---|---|---|---|---|---|---|---|---|
| | | $q_{e,calc}$ (mg $g^{-1}$) | $K_1$ ($min^{-1}$) | SD (%) | $R^2$ | $q_{e,calc}$ (mg $g^{-1}$) | $H$ (mg $g^{-1}$ $min^{-1}$) | $K_2$ (g $mg^{-1}$ $min^{-1}$) | SD (%) | $R^2$ |
| 50 | 19.589 | 2.468 | 0.0182 | 27.639 | 0.8728 | 19.786 | 10.595 | 0.0276 | 0.319 | 0.9999 |
| 100 | 32.346 | 11.539 | 0.0163 | 20.342 | 0.9281 | 34.161 | 11.024 | 0.0105 | 1.774 | 0.9999 |
| 150 | 57.271 | 16.645 | 0.0114 | 20.477 | 0.9576 | 56.593 | 12.216 | 0.0037 | 0.342 | 0.9999 |
| 200 | 73.421 | 25.549 | 0.0072 | 18.084 | 0.9632 | 75.930 | 13.462 | 0.0025 | 0.948 | 0.9993 |
| 250 | 85.308 | 28.839 | 0.0065 | 17.091 | 0.9455 | 86.281 | 14.184 | 0.0019 | 0.294 | 0.9996 |

of the particle at the beginning of adsorption. The above results suggested that the process can be best fitted by the pseudo-second-order rate equation and it can be an endothermic chemisorption. The adsorption experiments were performed at pH 1.8 and the zero potential charge of the adsorbent has been found to occur at pH 6.5. Hence at pH 1.8, the binding sites in the adsorbent were positively charged which promotes the attraction of negatively charged anionic dye molecules. The adsorption process was chemisorption involving strong binding forces via sharing or ion exchange of electrons among the adsorbent and adsorbate molecules as covalent forces [84]. The calculated value of $E_a$ and $\Delta H$ in the studied adsorption process again confirms the involvement of chemisorption mechanism as discussed in section 3.5. The rate constant, $K_2$, decreased from 0.0276 to $9.481 \times 10^{-4}$ g $mg^{-1}$ $min^{-1}$ with increase in adsorbate concentration from 50 to 250 mg $L^{-1}$. This may be due to increased competition at the active sites on the adsorbent surface at higher concentration and decreased competition for the binding sites at lower adsorbate concentrations [85].

### 3.7. Possible interactions between the RBBR dye and the GLP adsorbent

In order to understand the adsorption process of dye onto the GLP adsorbent, a mechanism of adsorption is essential. In fact, the process of adsorption is controlled by various factors such as nature of functional groups present in adsorbate and adsorbent, the structural and surface properties of the adsorbent, diffusion behavior of adsorbate towards the adsorbent, and the mode of their interaction. Indeed, the adsorption of dye occurs through physisorption or chemisorption, depending on the nature of mutual interaction between adsorbent surface and adsorbate. In many cases, the accumulation of dye on agricultural biomass materials happens due to the involvement of many interactions such as Π-Π interaction, electrostatic attraction, and hydrogen bonding, which can occur during the adsorption process. RBBR is an anionic dye that contains a sulfonic group in its structure, which ionizes in aqueous solution, forming colored anions, together with aromatic rings. The amount of ($-SO_3^-$) anions is an important factor for adsorption of RBBR. Agricultural materials particularly those containing cellulose show potential adsorption capacity for various pollutants. The major components present in the agricultural waste materials are cellulose, hemicellulose, lignin, lipids, proteins, and various functional groups. It may appears that the major mechanism of interactions between carbonaceous materials and adsorbate is the Π-Π stacking (most possible driving force for the adsorption of dyes is the Π-Π interaction between aromatic rings of GLP adsorbent and dye molecules). The proposed mechanism for adsorption of RBBR dye onto GLP adsorbent is shown in Fig. 16. ATR analysis demonstrated that the carbon surface of the adsorbent contain more hydroxyl, methyl, and carbonyl species. These groups may interact with the Π electron of the aromatic ring of the RBBR. Fig. 16 shows that the hydroxyl species getting involved in the binding of dye molecules on the surface of the adsorbent. A similar type of mechanism is also reported in the literature [86]. In addition, film diffusion and pore diffusion models have been most frequently used for examining their diffusion mechanism.

### 3.8. Inference from adsorption rate mechanism

The pore diffusion plot for the removal of RBBR onto the GLP adsorbent in three regions is shown in Fig. 17 and the model constants are given in Table S4. From Fig. 17, the first region follows the external film diffusion of the dye molecules and the process is rapid. It shows that the strong electrostatic interaction among adsorbate molecules and outer surface of the adsorbent. Second section is attributed to progressive adsorption stage, where intra-particle diffusion is rate controlling. It signifies the movement of adsorbate molecule through the pores [87]. The third region refers to the ultimate equilibrium stage and the pore diffusion starts to decrease due to the exceedingly low dye concentration in the aqueous solution [88]. Extrapolation of the second section back to the $y$ axis yields the value of $C$. A larger boundary layer diffusion effect is showed by a large intercept value. The decrease in intercept value denotes that the process is mainly controlled by pore diffusion, with a slight effect of external film diffusion. Also, the plots at each concentration do not pass through the origin, indicating that the pore diffusion was not only the rate limiting step [89]. The value of $K_i$ obtained from these plots increased with increase in initial adsorbate concentration. From Table S4, the value of $R^2$ of the pore diffusion model for various adsorbate concentrations was lower than pseudo-second-order kinetic model. This suggests that the experimental data were fitted with the pseudo-second-order kinetic model better. Therefore, the overall rate of the adsorption is mostly controlled by external boundary layer diffusion, followed by

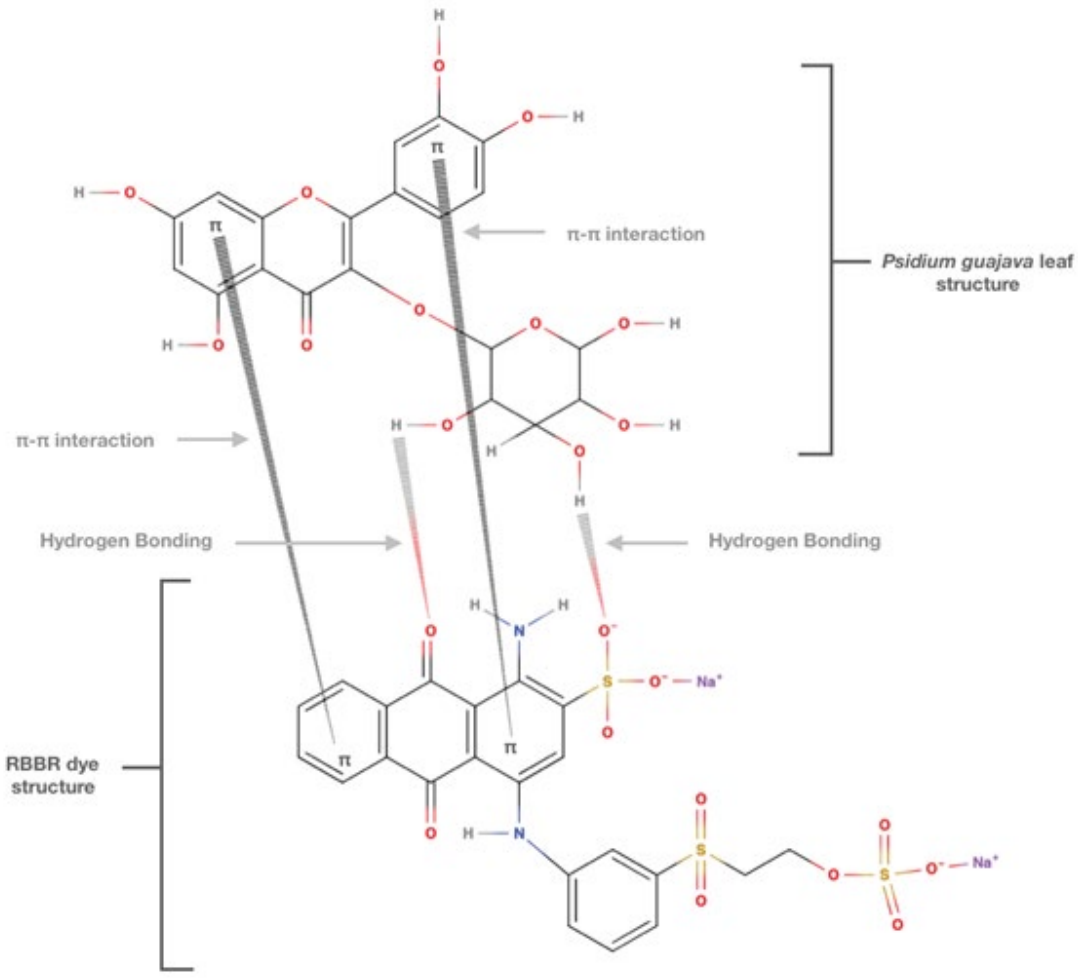


Fig. 16. Proposed mechanism for RBBR dye adsorption onto GLP adsorbent.

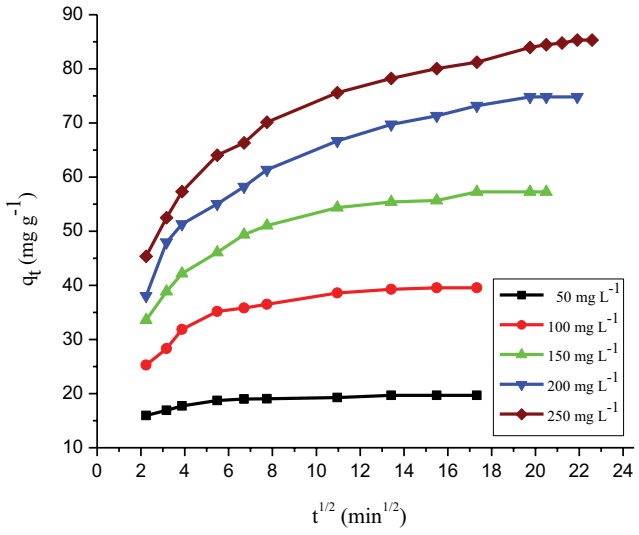


Fig. 17. Intra-particle diffusion plot for adsorption of RBBR dye onto GLP adsorbent (initial pH: 1.8; initial dye concentration: 50–250 mg $L^{-1}$; adsorbent dosage: 2.5 g $L^{-1}$; particle size: 125 μm; agitation speed: 150 rpm; contact time: 24 h).

a small effect of pore diffusion of RBBR dye anions to the particle interior surface. It was found that the adsorption process may be limited due to external boundary layer diffusion at initial stages and as the solid particles are accumulated with adsorbate molecules, it may be governed due to pore diffusion at subsequent stages [90]. The Bangham and Boyd kinetic expressions were used to further analyze the experimental data. The Boyd plot (Fig. 18) and Bangham plot (Fig. S9) were found to be a straight line that did not miss the origin and it suggests that the external boundary layer diffusion mostly controls the overall rate of the reaction.

### *3.9. Inference from desorption studies and reusability of GLP adsorbent*

Desorption experiments were performed for the removal of RBBR from GLP adsorbent and results are shown in Fig. S10 and Table S5. It exhibits that the measure of RBBR dye desorbed reduced with an increase in number of runs. The % desorption in all the runs was determined to be in the order of methanol > ethanol > 1 M NaOH > acetone with various desorbing reagents in separate batches. It was found that up to a maximum of 54.37% of the dye could be desorbed using

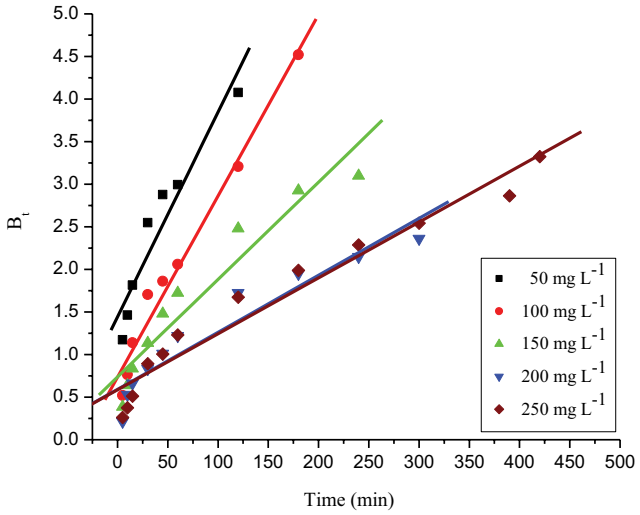


Fig. 18. Boyd plot for adsorption of RBBR dye onto GLP adsorbent (initial pH: 1.8; initial dye concentration: 50–250 mg $L^{-1}$; adsorbent dosage: 2.5 g $L^{-1}$; particle size: 125 μm; agitation speed: 150 rpm; contact time: 24 h).

the solvent methanol in the third run, compared with other desorbing reagents. This may be due to the low volume of the desorbing reagent used or lack of agitation speed, which may prevent further release of bound dye anions to the solvent [20].

The regenerated GLP adsorbent was added to the dye solution of concentration 200 mg $L^{-1}$. The regenerated adsorbent was tested in the second and third runs. The results obtained from reusability studies for the adsorption of RBBR in various runs are shown in Fig. S11 and Table S6. It shows that, in comparison with the first run, 80.46% adsorption was maintained after 24 h in the second run and 67.48% in the third run (using desorbing reagent methanol in the desorption process). This may be because of the incomplete desorption of the bound adsorbate molecules from the adsorbent binding sites (adsorbent active sites are almost blocked with RBBR dye molecules) and lack of vacant sites on the solid particle surface [13]. Therefore, the dye adsorption % gradually decreased with the increase in the number of runs.

## 4. Conclusion

The adsorption of RBBR using GLP adsorbent has been investigated in this study. The prepared adsorbent was characterized using ATR, SEM, BET and proximate analysis. The peaks in ATR studies revealed that the surface of the adsorbent material contains abundant hydroxyl, methyl, and carbonyl groups. Lower pH was found to favor the adsorption process. The % color removal of RBBR was found to decrease with increase in initial pH, adsorbate concentration and particle size. It increased with increase in adsorbent mass, and agitation speed. The adsorption capacity ($q_e$) improved as the initial adsorbate concentration increased. Higher temperature increased the adsorption, however the adsorption capacity $q_e$ reduced with increase in mass of adsorbent per L. The batch experiments were performed for the optimization of important process parameters using central composite design. The Langmuir model best fit the adsorption equilibrium suggesting monolayer adsorption. The pseudo-second-order kinetic model fitted the kinetic data best. The nature of the process was spontaneous and endothermic; thus higher temperatures favor the adsorption. The activation energy and change in enthalpy of adsorption suggests that the adsorption is a chemisorption process controlled by external boundary layer diffusion and it is the rate limiting step. Desorption studies on loaded adsorbent showed that the maximum % of RRBR dye could be desorbed using the solvent ethanol. It shows that the % desorption reduced with the total number of runs for all desorbing reagents. The regenerated adsorbent can be used effectively up to three cycles to adsorb RBBR dye in aqueous solutions in the absence of deprivation of adsorbent or considerable depletion in % color removal. The experimental results concluded that GLP is can be used as an excellent adsorbent for the removal of synthetic dye from wastewater. The better decolorization efficiency of synthetic dye effluent suggests that the guava leaf adsorbent may be used effectively to decolorize anionic dyes from industrial effluents.

### Symbols and abbreviations

| | | |
|---|---|---|
| $A$ | — | Arrhenius frequency factor |
| AAD | — | Absolute average deviation |
| Adj MS | — | Adjusted mean squares |
| Adj SS | — | Adjusted sum of squares |
| ANOVA | — | Analysis of variance |
| ATR | — | Attenuated transmission reflector |
| BET | — | Brunauer–Emmett–Teller |
| $B_t$ | — | Mathematical function of $F$ |
| $b_0$ | — | Offset term |
| $b_i$ | — | Regression coefficients for linear effect |
| $b_{ii}$ | — | Regression coefficients for quadratic effect |
| $b_{ij}$ | — | Regression coefficients for interaction effect |
| $b_T$ | — | Adsorption energy, kJ $mole^{-1}$ |
| $C$ | — | Constant, Intercept value |
| CCD | — | Central composite design |
| $C_0$ | — | Initial dye concentration in solution, mg $L^{-1}$ |
| $C_e$ | — | Equilibrium dye concentration in solution, mg $L^{-1}$ |
| $C_t$ | — | Dye concentration in solution at any time $t$, mg $L^{-1}$ |
| DF | — | Degree of freedom |
| $E_a$ | — | Activation energy of adsorption, kJ $mole^{-1}$ |
| EDS | — | Energy dispersive X-ray spectroscopy |
| $F$ | — | Ratio of amount of dye adsorbed at any time $t$ to equilibrium |
| $F_{statistics}$ | — | Fisher's F-test |
| $f$ | — | Number of variables |
| FESEM | — | Field emission scanning electron microscopy |
| $h$ | — | Initial rate of adsorption, g $g^{-1}$ $min^{-1}$ |
| $K_a$ | — | Adsorption equilibrium constant, L $g^{-1}$ |
| $K_F$ | — | Freundlich isotherm constant, L $g^{-1}$ |
| $K_i$ | — | Intra-particle diffusion rate constant, mg $g^{-1}$ $min^{-1/2}$ |
| $K_L$ | — | Langmuir isotherm constant, L $mg^{-1}$ |
| $K_T$ | — | Temkin isotherm constant, L $g^{-1}$ |
| $K_1$ | — | Pseudo-first-order rate constant, $min^{-1}$ |
| $K_2$ | — | Pseudo-second-order rate constant, g $mg^{-1}$ $min^{-1}$ |
| $k_0$ | — | Bangham constant, $L^2$ $g^{-1}$ |

MB — Methylene blue
$m$ — Mass of adsorbent per volume of solution, g $L^{-1}$
$N$ — Numbers of experimental runs
$N_P$ — Number of data points
$N_0$ — Center points
$n$ — Heterogeneity factor
$P$ — Probability value
PRESS — Predicted residual sum of squares
$q_e$ — Amount of dye adsorbed at equilibrium, mg $g^{-1}$
$q_{e,\text{expt}}$ — Experimental adsorption capacity, mg $g^{-1}$
$q_{e,\text{calc}}$ — Calculated adsorption capacity, mg $g^{-1}$
$q_{\max}$ — Theoretical monolayer maximum saturation capacity, mg $g^{-1}$
$q_t$ — Amount of dye adsorbed on the adsorbent surface at any time $t$, min
$R$ — Universal gas constant, 8.314 J $mole^{-1}$ $K^{-1}$
$R^2$ — Linear regression correlation coefficient
$R_L$ — Langmuir isotherm separation factor
RBBR — Remazol brilliant blue-R
RMSE — Root mean square error
RSM — Response surface methodology
$S$ — Value of $S$ chart
SD — Standard deviation
SE — Standard error
SEM — Scanning electron microscopy
Seq SS — Sequential sum of squares
$T_{\text{statistics}}$ — Student $T$-test
$t$ — Adsorption time, min
$T$ — Temperature, K
$V$ — Volume of dye solution, mL
$W$ — Mass of guava leaf adsorbent, g
$x_i$ — Dimensionless value of a process variable $X_i$
$X_i$ — Real value of an independent variable
$X_0$ — Value of $X_i$ at the center point
$X_1$ — Initial pH
$X_2$ — Initial dye concentration, mg $L^{-1}$
$X_3$ — Adsorbent dosage, g $L^{-1}$
$X_4$ — Adsorbent particle size, μm
$y_p$ — Predicted response variable
$y_a$ — Actual response variable
$\Delta G$ — Changes in Gibbs free energy, kJ $mole^{-1}$
$\Delta H$ — Changes in enthalpy, kJ $mole^{-1}$
$\Delta S$ — Changes in entropy, kJ $mole^{-1}$ $K^{-1}$
$2^f$ — Number of factorial points
$2f$ — Axial points

## Greek

$\alpha$ — Constant
$\delta X$ — Step change
$\chi^2$ — Chi-square test value

## References

[1] S.S. Mirzaee, E. Salahi, A. Khanlarkhani, Kinetics, isotherms and thermodynamic modeling of $Mn^{2+}$ and $Zn^{2+}$ single and binary removal using mercapto functionalized silica aerogel, J. Disper. Sci. Technol., 40 (2019) 657–667.
[2] M. Naushad, A.A. Alqadami, Z.A. AlOthman, I.H. Alsohaimi, M.S. Algamdi, A.M. Alawsari, Adsorption kinetics, isotherm and reusability studies for the removal of cationic dye from aqueous medium using arginine modified activated carbon, J. Mol. Liq., 293 (2019) 111442.
[3] M. Farnane, A. Elhalil, A. Machrouhi, F.Z. Mahjoubi, M. Sadiq, M. Abdennouri, S. Qourzal, H. Tounsadi, N. Barka, Enhanced adsorptive removal of cationic dyes from aqueous solution by chemically treated carob shells, Desal. Wat. Treat., 100 (2017) 204–213.
[4] C. Hu, N. Hu, X. Li, H. Shen, Y. Zhao, Adsorption of Remazol brilliant blue-R by carboxylated multi-walled carbon nanotubes, Desal. Wat. Treat., 62 (2017) 282–289.
[5] K. Ada, A. Ergene, S. Tan, E. Yalcin, Adsorption of Remazol brilliant blue-R using ZnO fine powder: equilibrium, kinetic and thermodynamic modeling studies, J. Hazard. Mater., 165 (2009) 637–644.
[6] M.A. Ahmad, N. Ahmad, O.S. Bello, Removal of Remazol brilliant blue reactive dye from aqueous solutions using watermelon rinds as adsorbent, J. Disper. Sci. Technol., 36 (2015) 845–858.
[7] M.A. Ahmad, S.G. Herawan, A.A. Yusof, Equilibrium, kinetics, and thermodynamics of Remazol brilliant blue-R dye adsorption onto activated carbon prepared from pinang frond, Int. Sch. Res. Notices, 2014 (2014) 1–7.
[8] A. Machrouhi, A. Elhalil, M. Farnane, F.Z. Mahjoubi, H. Tounsadi, M. Sadiq, M. Abdennouri, N. Barka, Adsorption behavior of methylene blue onto powdered *Ziziphus lotus* fruit peels and Avocado kernels seeds, J. Appl. Surf. Interfaces, 1 (2017) 49–56.
[9] Z.A. Medvedev, H.M. Crowne, M.N. Medvedeva, Age related variations of hepatocarcinogenic effect of azo dye (3′- MDAB) as linked to the level of hepatocyte polyploidization, Mech. Ageing Dev., 46 (1988) 159–174.
[10] E. Daneshvar, A. Vazirzadeh, A. Niazi, M. Kousha, M. Naushad, A. Bhatnagar, Desorption of Methylene blue dye from brown macroalga: effects of operating parameters, isotherm study and kinetic modeling, J. Clean. Prod., 152 (2017) 443–453.
[11] A.A. Markadeh, A. Rezaee, S.O. Rastegar, H. Hossini, S. Ahmadi, E. Hoseinzadeh, Optimization of Remazol brilliant blue adsorption process from aqueous solutions using multi-walled carbon nanotube, Desal. Wat. Treat., 57 (2016) 13357–13365.
[12] N. Mathur, P. Bhatnagar, P. Bakre, Assessing mutagenicity of textile dyes from Pali (Rajasthan) using AMES bioassay, Appl. Ecol. Environ. Res., 4 (2005) 111–118.
[13] P. Vairavel, V.R. Murty, Continuous fixed-bed adsorption of Congo red dye by dual adsorbent (*Neurospora crassa* dead fungal biomass and wheat bran): experimental and theoretical breakthrough curves, immobilization and reusability studies, Desal. Wat. Treat., 98 (2017) 276–293.
[14] A.B. Albadarin, M.N. Collins, M. Naushad, S. Shirazian, G. Walker, C. Mangwandi, Activated lignin-chitosan extruded blends for efficient adsorption of methylene blue, Chem. Eng. J., 307 (2017) 264–272.
[15] M. Naushad, G. Sharma, Z.A. Alothman, Photodegradation of toxic dye using Gum Arabic-cross linked-poly(acrylamide)/Ni(OH)2/FeOOH nanocomposites hydrogel, J. Clean. Prod., 241 (2019) 118263.
[16] M. Abbas, T. Aksil, M. Trari, Removal of toxic methyl green (MG) in aqueous solutions by apricot stone activated carbon – equilibrium and isotherms modelling, Desal. Wat. Treat., 125 (2018) 93–101.
[17] P. Vairavel, V.R. Murty, Optimization, kinetics, equilibrium isotherms and thermodynamics studies for Congo red dye adsorption using calcium alginate beads immobilized with dual adsorbent (*Neurospora crassa* dead fungal biomass and wheat bran), Desal. Wat. Treat., 97 (2017) 338–362.
[18] S. Zafar, M.I. Khan, M. Khraisheh, S. Shahida, T. Javed, M.L. Mirza, N. Khalid, Use of rice husk as an effective sorbent for the removal of cerium ions from aqueous solution: kinetic, equilibrium and thermodynamic studies, Desal. Wat. Treat., 150 (2019) 124–135.
[19] V.K. Gupta, Suhas, Application of low-cost adsorbents for dye removal – a review, J. Environ. Manage., 90 (2009) 2313–2342.

[20] P. Vairavel, V.R. Murty, S. Nethaji, Removal of Congo red dye from aqueous solutions by adsorption onto a dual adsorbent (*Neurospora crassa* dead biomass and wheat bran): optimization, isotherm, and kinetics studies, Desal. Wat. Treat., 68 (2017) 274–292.
[21] R. Han, W. Zou, W. Yu, S. Cheng, Y. Wang, J. Shi, Biosorption of Methylene blue from aqueous solution by fallen phoenix tree's leaves, J. Hazard. Mater., 141 (2007) 156–162.
[22] K.V. Kumar, A. Kumaran, Removal of Methylene blue by mango seed kernel powder, Biochem. Eng. J., 27 (2005) 83–93.
[23] Sumanjit, T.P.S. Walia, R. Kaur, Removal of health hazards causing acidic dyes from aqueous solutions by the process of adsorption, Online J. Health Allied Sci., 3 (2007) 1–10.
[24] K.G. Bhattacharyya, A. Sharma, *Azadirachta indica* leaf powder as an effective biosorbent for dyes: a case study with aqueous Congo red solutions, J. Environ. Manage., 71 (2004) 217–229.
[25] V. Ponnusami, S. Vikram, S.N. Srivastava, Guava (*Psidium guajava*) leaf powder: novel adsorbent for removal of Methylene blue from aqueous solutions, J. Hazard. Mater., 152 (2008) 276–286.
[26] C. Anthony, A review of Guava (*Psidium guajava*), Personal Care Mag., 6 (2005) 33–39.
[27] A. Weli, A. Al-Kaabi, J. Al-Sabahi, S. Said a, M.A. Hossain, S. Al-Riyami, Chemical composition and biological activities of the essential oils of *Psidium guajava* leaf, J. King Saud Univ. Sci., 2018. doi:10.1016/j.jksus.2018.07.021.
[28] V.S. Mane, P.V.V. Babu, Kinetic and equilibrium studies on the removal of Congo red from aqueous solution using Eucalyptus wood (*Eucalyptus globulus*) saw dust, J. Taiwan Inst. Chem. Eng., 44 (2013) 81–88.
[29] M.T. Sulak, E. Demirbas, M. Kobya, Removal of Astrazon yellow 7GL from aqueous solutions by adsorption onto wheat bran, Bioresour. Technol., 98 (2007) 2590–2598.
[30] P. Vairavel, V.R. Murty, Optimization of batch process parameters for Congo red color removal by *Neurospora crassa* live fungal biomass with wheat bran dual adsorbent using response surface methodology, Desal. Wat. Treat., 103 (2018) 84–101.
[31] G.M. Ratnamala, K.V. Shetty, G. Srinikethan, Isotherm, kinetics, and process optimization for removal of Remazol brilliant blue dye from contaminated water using adsorption on acid-treated red mud, Desal. Wat. Treat., 57 (2016) 11361–11374.
[32] M.R. Sohrabi, S. Amiri, H.R.F. Masoumi, M. Moghri, Optimization of Direct yellow 12 dye removal by nanoscale zero-valent iron using response surface methodology, J. Ind. Eng. Chem., 20 (2014) 2535–2542.
[33] I.A.W. Tan, B.H. Hameed, A.L. Ahmad, Equilibrium and kinetic studies on basic dye adsorption by oil palm fibre activated carbon, Chem. Eng. J., 127 (2007) 111–119.
[34] H.M.F. Freundlich, Over the adsorption in solution, J. Phys. Chem., 385 (1906) 385–470.
[35] V.K. Gupta, R. Jain, S. Varshney, Removal of reactofix golden yellow 3 RFN from aqueous solution using wheat huskan agricultural waste, J. Hazard. Mater., 142 (2007) 443–448.
[36] M.A. Ahmad, N.K. Rahman, Equilibrium, kinetics and thermodynamics of Remazol brilliant orange 3R dye adsorption on coffee husk-based activated carbon, Chem. Eng. J., 170 (2011) 154–161.
[37] I. Langmuir, The adsorption of gases on plane surfaces of glass, mica and platinum, J. Am. Chem. Soc., 40 (1918) 1361–1403.
[38] K.R. Hall, L.C. Eagleton, A. Acrivos, T. Vermeulen, Pore and solid diffusion kinetics in fixed-bed adsorption under constant pattern conditions, Ind. Eng. Chem. Fundam., 5 (1966) 212–223.
[39] S. Karaca, A. Gurses, O. Acisli, A. Hassani, M. Kiransan, K. Yikilmaz, Modeling of adsorption isotherms and kinetics of Remazol red RB adsorption from aqueous solution by modified clay, Desal. Wat. Treat., 51 (2013) 2726–2739.
[40] M.J. Temkin, V. Pyzhev, Kinetics of ammonia synthesis on promoted iron catalysts, Acta Physicochim. U.R.S.S., 12 (1940) 217–222.
[41] V.S. Munagapati, D.S. Kim, Adsorption of anionic azo dye Congo Red from aqueous solution by cationic modified orange peel powder, J. Mol. Liq., 220 (2016) 540–548.
[42] B.H. Hameed, A.A. Ahmad, N. Aziz, Isotherms, kinetics and thermodynamics of acid dye adsorption on activated palm ash, Chem. Eng. J., 133 (2007) 195–203.
[43] S. Kaur, S. Rani, R.K. Mahajan, Adsorption kinetics for the removal of hazardous dye Congo red by bio-waste materials as adsorbents, J. Chem., 2013 (2013) 1–12.
[44] V.S. Munagapati, D.S. Kim, Equilibrium isotherms, kinetics, and thermodynamics studies for Congo red adsorption using calcium alginate beads impregnated with nano-goethite, Ecotoxicol. Environ. Saf., 141 (2017) 226–234.
[45] L. Abramian, H. EI-Rassy, Adsorption kinetics and thermodynamics of azo-dye Orange II onto highly titania aerogel, Chem. Eng. J., 150 (2009) 403–410.
[46] V.K. Gupta, D. Pathania, S. Sharma, S. Agarwal, P. Singh, Remediation and recovery of Methyl orange from aqueous solution onto acrylic acid grafted ficus carica fiber: Isotherms, kinetics and thermodynamics, J. Mol. Liq., 177 (2013) 325–334.
[47] M. Dogan, H. Abak, M. Alkan, Adsorption of methylene blue onto hazelnut shell: kinetics, mechanism and activation parameters, J. Hazard. Mater., 164 (2009) 172–181.
[48] S.S. Gupta, K.G. Bhattacharyya, Kinetics of adsorption of metal ions on inorganic materials: a review, Adv. Colloid Interface Sci., 162 (2011) 39–58.
[49] S. Lagergren, Zur theorie der sogenannten adsorption geloster stoffe, K. Sven. Vetenskapsakad. Handl., 24 (1898) 1–39.
[50] Y.S. Ho, G. McKay, Pseudo-second order model for sorption processes, Process Biochem., 34 (1999) 451–465.
[51] R. Elangovan, L. Philip, K. Chandraraj, Biosorption of hexavalent and trivalent chromium by palm flower (*Borassus aethiopum*), Chem. Eng. J., 141 (2008) 99–111.
[52] D. Pathania, A. Sharma, Z.M. Siddiqi, Removal of Congo red dye from aqueous system using *Phoenix dactylifera* seeds, J. Mol. Liq., 219 (2016) 359–367.
[53] Y. El-Mouzdahir, A. Elmchaouri, R. Mahboub, A. El-Anssari, A. Gil, S.A. Korili, M.A. Vicente, Interaction of stevensite with $Cd^{2+}$ and $Pb^{2+}$ in aqueous dispersions, Appl. Clay Sci., 35 (2007) 47–58.
[54] A. Gurses, C. Dogar, M. Yalcin, M. Acikyildiz, R. Bayrak, S. Karaca, The adsorption kinetics of the cationic dye, Methylene blue, onto clay, J. Hazard. Mater., 131 (2006) 217–228.
[55] V. Vadivelan, K.V. Kumar, Equilibrium, kinetics, mechanism, and process design for the sorption of methylene blue onto rice husk, J. Colloid Interface Sci., 286 (2005) 90–100.
[56] V.K. Gupta, I. Ali, Suhas, V.K. Saini, Adsorption of 2,4-D and carbofuran pesticides using fertilizer and steel industry wastes, J. Colloid Interface Sci., 299 (2006) 556–563.
[57] F. Raposo, M.A.D.L. Rubia, R. Borja, Methylene blue number as useful indicator to evaluate the adsorptive capacity of granular activated carbon in batch mode: influence of adsorbate/adsorbent mass ratio and particle size, J. Hazard. Mater., 165 (2009) 291–299.
[58] ASTM (2006) Standard Test Method for Determination of Iodine Number of Activated Carbon. D4607–94.
[59] F.O. Nwosu, O.J. Ajala, R.M. Owoyemi, B.G. Raheem, Preparation and characterization of adsorbents derived from bentonite and kaolin clays, Appl. Water Sci., 8 (2018) 195–204.
[60] M. Rajib, C.T. Oguchi, S.M.M. Hasan, In-situ oxidation effect on pore size distribution in investigating adsorption properties under various geochemical conditions, Solid Earth Sci., 4 (2019) 113–124.
[61] P.C. Jain, M. Jain, Engineering Chemistry (Chemistry of Engineering Materials), 9th edition, Dhanpat Rai & Sons Publishing Company Ltd., India, 1992.
[62] B.H. Stuart, Infrared Spectroscopy: Fundamentals and Applications, John Wiley & Sons Ltd., New York, USA, 2004.
[63] L.S. Krishna, K. Soontarapa, N.K. Asmel, M.A. Kabir, A. Yuzir, W.Y.W. Zuhairi, Y. Sarala, Adsorption of acid blue 25 from aqueous solution using zeolite and surfactant modified zeolite, Desal. Wat. Treat., 150 (2019) 348–360.
[64] Z.A. AL-Othman, R. Ali, M. Naushad, Hexavalent chromium removal from aqueous medium by activated carbon prepared from peanut shell: adsorption kinetics, equilibrium and thermodynamic studies, Chem. Eng. J., 184 (2012) 238–247.

[65] A.A. Alqadami, M. Naushad, M.A. Abdalla, M.R. Khan, Z.A. Alothman, Adsorptive removal of toxic dye using $Fe_3O_4$–TSC nanocomposite: equilibrium, kinetic, and thermodynamic studies, J. Chem. Eng. Data, 61 (2016) 3806–3813.
[66] T. Tatarchuk, N. Paliychuk, R.B. Bitra, A. Shyichuk, M. Naushad, I. Mironyuk, D. Ziołkowska, Adsorptive removal of toxic Methylene Blue and Acid Orange 7 dyes from aqueous medium using cobalt-zinc ferrite nanoadsorbents, Desal. Wat. Treat., 150 (2019) 374–385.
[67] K. Ravikumar, K. Pakshirajan, T. Swaminathan, K. Balu, Optimization of batch process parameters using response surface methodology for dye removal by a novel adsorbent, Chem. Eng. J., 105 (2005) 131–138.
[68] K.K. Wong, C.K. Lee, K.S. Low, M.J. Haron, Removal of Cu and Pb by tartaric acid modified rice husk from aqueous solutions, Chemosphere, 50 (2003) 23–28.
[69] D. Montgomery, G.C. Runger, Applied Statistics and Probability for Engineers, 5th edn., John Wiley & Sons Ltd. New York, USA, 2011.
[70] N.A. Rahmat, A.A. Ali, N. Hussain, M.S. Muhamad, R.A. Kristanti, T. Hadibarata, Removal of Remazol brilliant blue-R from aqueous solution by adsorption using pineapple leaf powder and lime peel powder, Water Air Soil Pollut., 227 (2016) 1–11.
[71] M.R. Mafra, L. Igarashi-Mafra, D.R. Zuim, E.C. Vasques, M.A. Ferreira, Adsorption of remazol brilliant blue on an orange peel adsorbent, Braz. J. Chem. Eng., 30 (2013) 657–665.
[72] A. Kuleyin, F. Aydin, Removal of reactive textile dyes (Remazol brilliant blue-R and Remazol yellow) by surfactant-modified natural zeolite, Environ. Progr. Sustain. Energy, 30 (2011) 141–151.
[73] K.C. Bedin, S.P.D. Azevedo, P.K.T. Leandro, A.L. Cazetta, V.C. Almeida, Bone char prepared by $CO_2$ atmosphere: preparation optimization and adsorption studies of Remazol brilliant blue-R, J. Clean. Prod., 161 (2017) 288–298.
[74] S. Dagdelen, B. Acemioglu, E. Baran, O. Kocer, Removal of Remazol brilliant blue-R from aqueous solution by pirina pretreated with nitric acid and commercial activated carbon, Water Air Soil Pollut., 225 (2014) 1–15.
[75] G.M. Ratnamala, K.V. Shetty, G. Srinikethan, Removal of Remazol brilliant blue dye from dye-contaminated water by adsorption using red mud: equilibrium, kinetic, and thermodynamic studies, Water Air Soil Pollut., 223 (2012) 6187–6199.
[76] V. Janaki, B.T. Oh, K. Shanthi, K.J. Lee, A.K. Ramasamy, S. Kamala-Kannan, Polyaniline/chitosan composite: an eco-friendly polymer for enhanced removal of dyes from aqueous solution, Synth. Met., 162 (2012) 974–980.
[77] M.R. Kulkarni, C. Bhagyalakshmi, D. Anand, R.N. Herle, Removal of Remazol brilliant blue dye from aqueous solutions using water hyacinth root powder, Desal. Wat. Treat., 122 (2018) 331–338.
[78] U. Gecgel, H. Kolancilar, Adsorption of Remazol brilliant blue-R on activated carbon prepared from a pine cone, Nat. Prod. Res., 26 (2012) 659–664.
[79] B.T. Pelosi, L.K.S. Lima, M.G.A. Vieira, Removal of the synthetic dye Remazol brilliant blue-R from textile industry wastewaters by biosorption on the macrophyte *Salvinia natans*, Braz. J. Chem. Eng., 31 (2014) 1035–1045.
[80] A. Ergene, K. Ada, S. Tan, H. Katircioglu, Removal of Remazol brilliant blue-R dye from aqueous solutions by adsorption onto immobilized *Scenedesmus quadricauda*: equilibrium and kinetic modeling studies, Desalination, 249 (2009) 1308–1314.
[81] S.L. Chan, Y.P. Tan, A.H. Abdullah, S.T. Ong, Equilibrium, kinetic and thermodynamic studies of a new potential biosorbent for the removal of basic blue 3 and congo red dyes: Pineapple (*Ananas comosus*) plant stem, J. Taiwan Inst. Chem. Eng., 61 (2016) 306–315.
[82] N.K. Amin, Removal of reactive dye from aqueous solutions by adsorption onto activated carbons prepared from sugarcane bagasse pith, Desalination, 223 (2008) 152–161.
[83] W. Konicki, A. Hełminiak, W. Arabczyk, E. Mijowska, Removal of anionic dyes using magnetic Fe@graphite core-shell nanocomposite as an adsorbent from aqueous solutions, J. Colloid Interface Sci., 497 (2017) 155–164.
[84] I.D. Mall, V.C. Srivastava, N.K. Agarwal, I.M. Mishra, Removal of Congo red from aqueous solution by bagasse fly ash and activated carbon: kinetic study and equilibrium isotherm analyses, Chemosphere, 61 (2005) 492–501.
[85] Y. Feng, D.D. Dionysiou, Y. Wu, H. Zhou, L. Xue, S. He, L. Yang, Adsorption of dyestuff from aqueous solutions through oxalic acid-modified swede rape straw: adsorption process and disposal methodology of depleted bioadsorbents, Bioresour. Technol., 138 (2013) 191–197.
[86] R.A. Reza, M. Ahmaruzzaman, A novel synthesis of $Fe_2O_3$@ activated carbon composite and its exploitation for the elimination of carcinogenic textile dye from an aqueous phase, RSC Adv., 5 (2015) 10575–10586.
[87] B.H. Hameed, M.I. El-Khaiary, Equilibrium, kinetics and mechanism of Malachite green adsorption on activated carbon prepared from bamboo by $K_2CO_3$ activation and subsequent gasification with $CO_2$, J. Hazard. Mater., 157 (2008) 344–351.
[88] L. Wang, J. Zhang, R. Zhao, C. Li, Y. Li, C. Zhang, Adsorption of basic dyes on activated carbon prepared from *Polygonum orientale* Linn: equilibrium, kinetic and thermodynamic studies, Desalination, 254 (2010) 68–74.
[89] D. Ozer, G. Dursun, A. Ozer, Methylene blue adsorption from aqueous solution by dehydrated peanut hull, J. Hazard. Mater., 144 (2007) 171–179.
[90] V. Ponnusami, K.S. Rajan, S.N. Srivastava, Application of film-pore diffusion model for Methylene blue adsorption onto plant leaf powders, Chem. Eng. J., 163 (2010) 236–242.

## Supplementary information

Table S1
Proximate analysis of GLP adsorbent

| Parameters | Values (%) |
|---|---|
| Moisture content | 7.62 |
| Volatile matter | 67.34 |
| Ash content | 6.50 |
| Fixed carbon | 18.54 |

Table S2
Chemical characterization of GLP before and after adsorption

| Process mode | Elements (weight %) | | | |
|---|---|---|---|---|
| | Carbon | Oxygen | Silicon | Calcium |
| Before adsorption | 47.34 | 51.22 | 0.16 | 1.28 |
| After adsorption | 48.12 | 51.45 | – | – |

Table S3
Activation energy for the adsorption of RBBR dye onto GLP adsorbent at various initial dye concentrations

| Initial dye concentration (mg $L^{-1}$) | Activation energy, $E_a$ (kJ $mole^{-1}$) |
|---|---|
| 50 | 60.931 |
| 100 | 67.012 |
| 150 | 66.178 |
| 200 | 67.262 |
| 250 | 63.805 |

Table S4
Kinetic model constants for intra-particle diffusion at different initial RBBR dye concentrations

| Initial dye concentration, $C_0$ (mg $L^{-1}$) | Intra-particle diffusion model | | |
|---|---|---|---|
| | $K_i$ (mg $g^{-1}$ $min^{-1/2}$) | $C$ | $R^2$ |
| 50 | 0.080 | 18.406 | 0.9599 |
| 100 | 0.397 | 33.407 | 0.9584 |
| 150 | 0.321 | 50.997 | 0.9527 |
| 200 | 0.940 | 55.900 | 0.9687 |
| 250 | 0.859 | 66.515 | 0.9954 |

Table S5
Desorption studies for the removal of RBBR dye from GLP adsorbent in various runs

| Sl. No | Desorbing reagent | % Desorption of RBBR dye from GLP adsorbent | | |
|---|---|---|---|---|
| | | 1st run | 2nd run | 3rd run |
| 1 | Methanol | 83.482 | 72.237 | 54.366 |
| 2 | Ethanol | 72.637 | 57.31 | 38.774 |
| 3 | Acetone | 57.839 | 38.781 | 20.454 |
| 4 | 1 M NaOH | 66.792 | 46.504 | 33.637 |

Table S6
Reusability of GLP adsorbent for the adsorption of RBBR dye in various runs

| Sl. No | Desorbing reagent | % Adsorption of RBBR dye by regenerated GLP adsorbent | | |
|---|---|---|---|---|
| | | 1st run | 2nd run | 3rd run |
| 1 | Methanol | 94.486 | 80.467 | 67.477 |
| 2 | Ethanol | 94.439 | 66.402 | 52.271 |
| 3 | Acetone | 94.486 | 45.654 | 30.748 |
| 4 | 1 M NaOH | 94.533 | 54.019 | 42.397 |

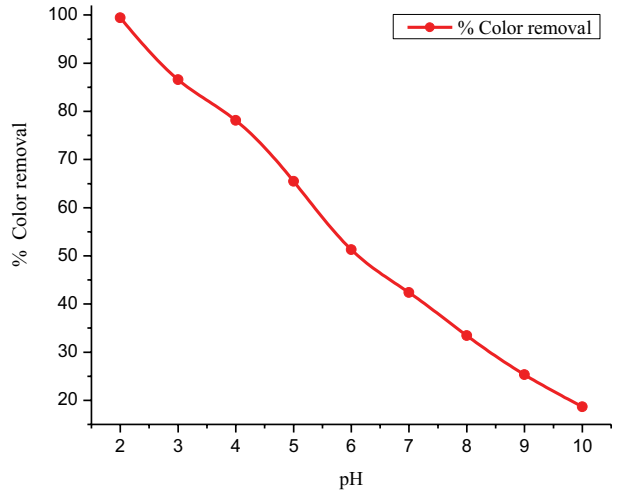


Fig. S1. Effect of initial pH on removal of RBBR dye by GLP adsorbent (initial dye concentration: 100 mg $L^{-1}$; adsorbent dosage: 5 g $L^{-1}$; adsorbent particle size: 105 μm; agitation speed: 150 rpm; temperature: 303 K; contact time: 6 h).

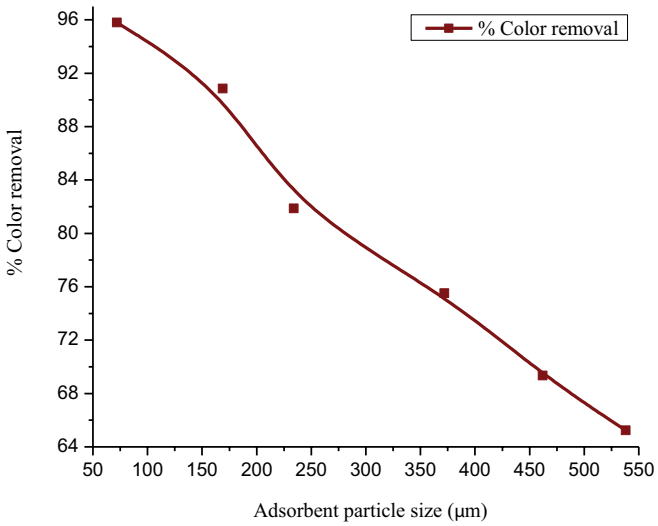


Fig. S2. Effect of GLP adsorbent particle size on RBBR dye adsorption (initial pH: 2; initial dye concentration: 100 mg $L^{-1}$; adsorbent dosage: 2 g $L^{-1}$; agitation speed: 150 rpm; temperature: 303 K; contact time: 6 h).

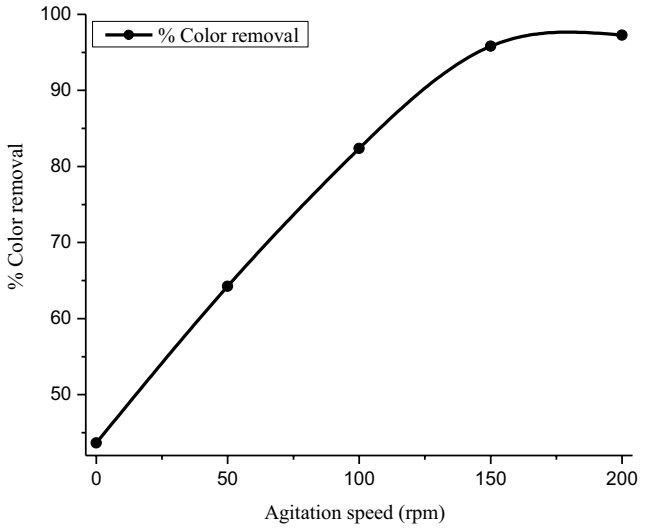


Fig. S3. Effect of agitation speed on removal of RBBR dye by GLP adsorbent (initial pH: 6; initial dye concentration: 100 mg $L^{-1}$; adsorbent dosage: 2 g $L^{-1}$; adsorbent particle size: 72 μm; temperature: 303 K; contact time: 6 h).

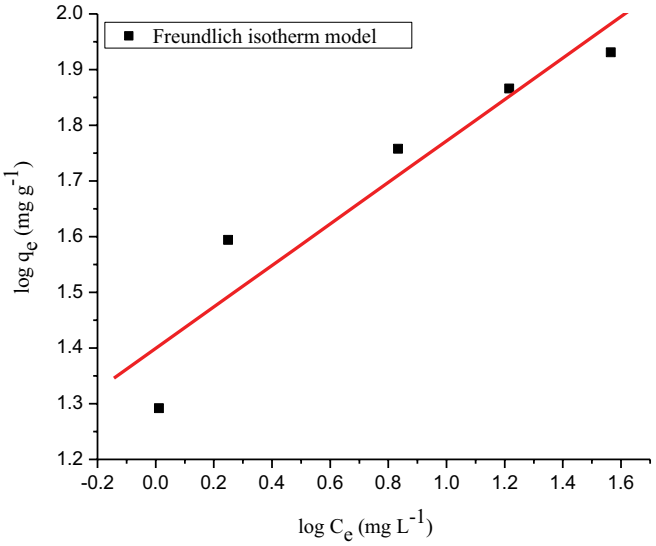


Fig. S4. Freundlich isotherm plot for adsorption of RBBR dye onto GLP adsorbent (initial pH: 1.8; initial dye concentration: 50–250 mg $L^{-1}$; adsorbent dosage: 2.5 g $L^{-1}$; particle size: 125 μm; agitation speed: 150 rpm; temperature: 303 K; contact time: 24 h).

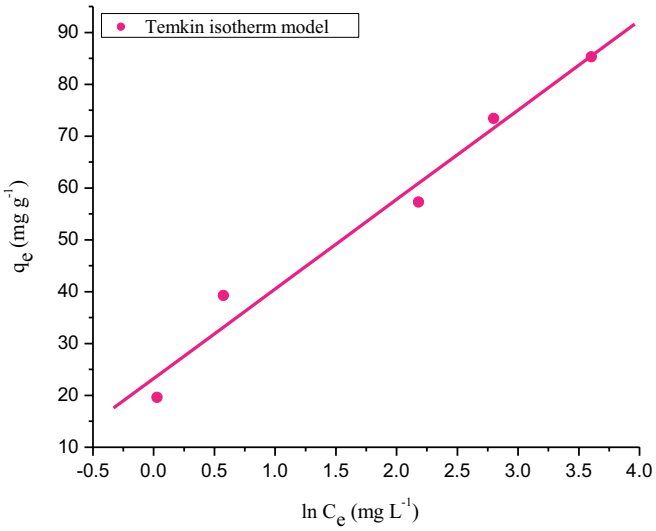


Fig. S5. Temkin isotherm plot for adsorption of RBBR dye onto GLP adsorbent (initial pH: 1.8; initial dye concentration: 50–250 mg $L^{-1}$; adsorbent dosage: 2.5 g $L^{-1}$; particle size: 125 μm; agitation speed: 150 rpm; temperature: 303 K; contact time: 24 h).

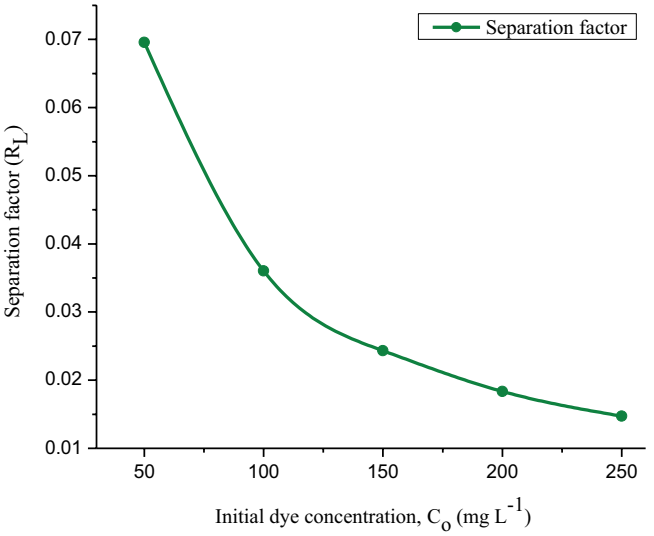


Fig. S6. Separation factor for adsorption of RBBR dye onto GLP adsorbent (initial pH: 1.8; initial dye concentration: 50–250 mg $L^{-1}$; adsorbent dosage: 2.5 g $L^{-1}$; particle size: 125 μm; agitation speed: 150 rpm; temperature: 303 K; contact time: 24 h).

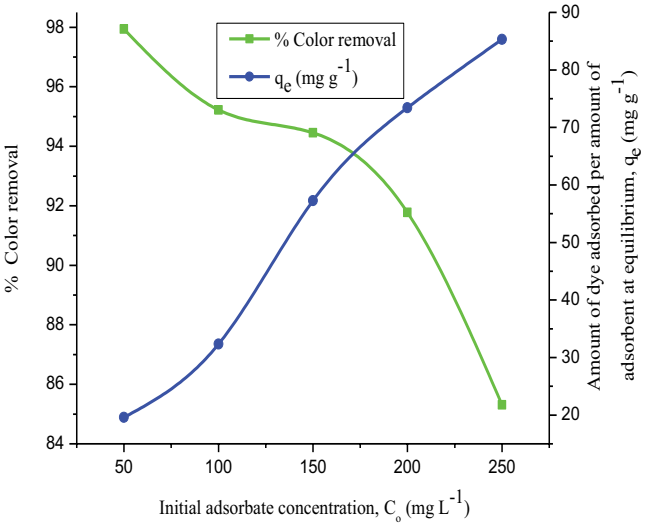


Fig. S7. Effect of initial dye concentration on removal of RBBR dye by GLP adsorbent (initial pH: 1.8; adsorbent dosage: 2.5 g $L^{-1}$; adsorbent particle size: 125 μm; agitation speed: 150 rpm; temperature: 303 K; contact time: 24 h).

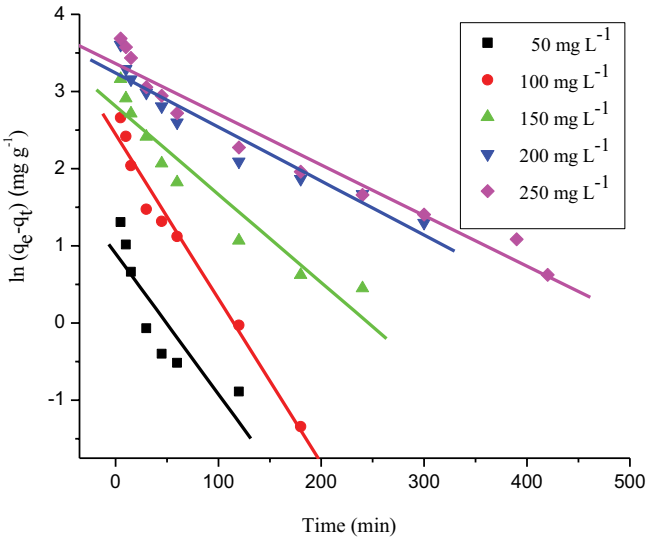


Fig. S8. Lagergren pseudo-first-order kinetic plot for adsorption of RBBR dye onto GLP adsorbent (initial pH: 1.8; initial dye concentration: 50–250 mg $L^{-1}$; adsorbent dosage: 2.5 g $L^{-1}$; particle size: 125 μm; agitation speed: 150 rpm; temperature: 303 K; contact time: 24 h).

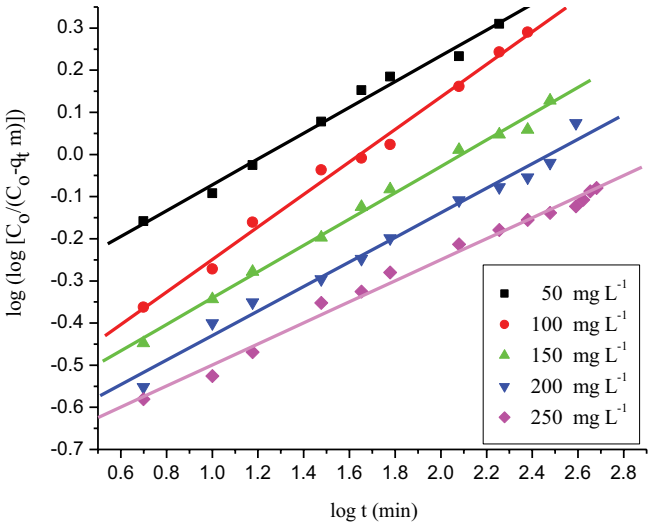


Fig. S9. Bangham plot for adsorption of RBBR dye onto GLP adsorbent (initial pH: 1.8; initial dye concentration: 50–250 mg $L^{-1}$; adsorbent dosage: 2.5 g $L^{-1}$; particle size: 125 μm; agitation speed: 150 rpm; temperature: 303 K; contact time: 24 h).

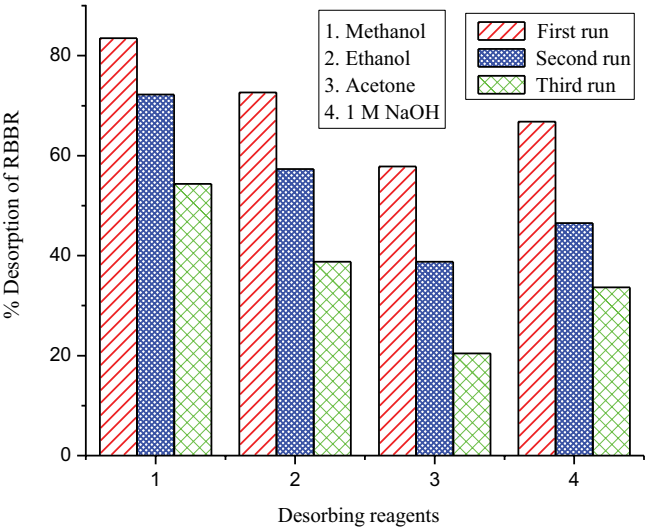


Fig. S10. Desorption efficiency of RBBR dye from GLP adsorbent in various runs (volume of desorbing reagent: 100 mL; shaking speed: 150 rpm; temperature: 303 K; contact time: 24 h).

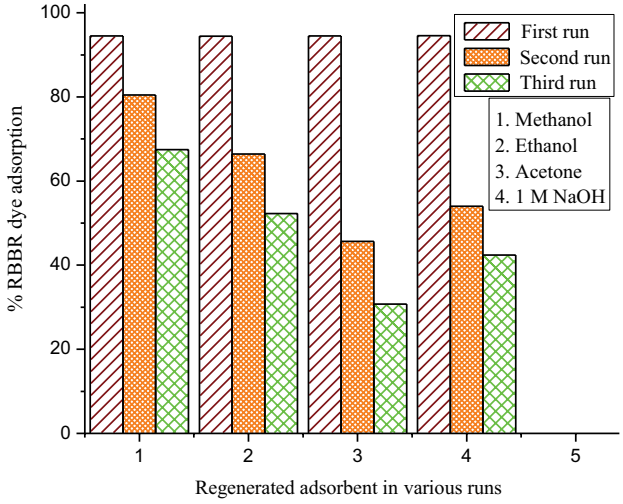


Fig. S11. Reusability of GLP adsorbent for the adsorption of RBBR dye in various runs (initial pH: 1.8; initial dye concentration: 200 mg $L^{-1}$; volume of dye solution: 100 mL; agitation speed: 150 rpm; temperature: 303 K; contact time: 24 h).